



Cascade feedforward neural network and deep neural network controller on photovoltaic system with cascaded multilevel inverters: Comparison on standalone and grid integrated system

Mailugundla Rupesh ^{a, *}, Vishwanath Shivalingappa Tegampure ^b

^a Department of Electrical & Electronics Engineering, BVRIT Hyderabad College of Engineering for Women Bachupally, 8-5/4, Nizampet Rd, Opposite Rajiv Gandhi Nagar Colony, Hyderabad, Telangana 500090, India

^b Department of Electronics & Communication Engineering, Bheemanna Khandre Institute of Technology 26M6+HM9, Bhalki-Humnabad Road, Bhalki, Bidar, Karnataka 585328, India

Received 18 May 2022; Revised 11 August 2022; Accepted 5 September 2022; Published online 29 December 2022

Abstract

The introduction of a micro-grid-based power generation network will help to meet the demands of consumers while reducing environmental impact. Several industrialized and emerging countries allocate considerable resources to renewable energy-based power generation and invest significant sums of money in this area. This study examines the challenges involved with electricity generation through photovoltaic (PV) systems and the integration of the same with the grid to mitigate power quality issues and improve the power factor for various loading conditions. An innovative multilevel inverter for grid-connected PV systems has been developed to enhance the voltage profile and resulted in a drop in total harmonic distortion (THD). A cascade multilevel inverter (associated with a grid-integrated PV system and managed using multiple innovative artificial intelligence controllers) was developed in this research project. Various advanced intelligent controllers, such as cascade feedforward neural networks (CFFNN) and deep neural networks (DNN), have been analyzed under various operating situations and observed that the THD of voltage, current at the grid, and the load is less than 3 % as per the IEEE 519 standards along with this power factor is maintained nearly unity for the grid-connected system. The quality of power in terms of voltage, frequency, total harmonics distortion, and power factor are improved by using a novel deep neural network algorithm in a cascaded multilevel inverter and verified according to IEEE 1547 and IEEE 519 standards to determine the efficacy of the proposed system.

Copyright ©2022 National Research and Innovation Agency. This is an open access article under the CC BY-NC-SA license (<https://creativecommons.org/licenses/by-nc-sa/4.0/>).

Keywords: cascaded feedforward neural network; deep neural network; multilevel inverter; photovoltaic system; total harmonics distortion.

I. Introduction

Over the past 20 years, renewable energy has gained widespread recognition. Future power-generating technologies are anticipated to be competitive with renewable energy sources [1]. Increased efforts have been made to employ renewable energy sources more frequently rather than polluting fossil fuels and other energy sources.

Alternative energy sources have recently attracted a lot of interest, including photovoltaic (PV), hydro, fuel, and wind power generation systems. To fulfill the growing energy demand and stop climate change, the usage of renewable energy has been accelerated swiftly [1][2].

The two different kinds of PV power generating applications are off-grid and grid-integrated systems. An off-grid system is best suited for low-power applications and needs a battery to accumulate PV energy [3]. A grid-connected system, on the other hand, is the most economical choice for high-power

* Corresponding Author. Tel: Tel: +91-9985755453
E-mail address: m.rupesh1@gmail.com

applications since it doesn't need a battery bank. Compared to other renewable energy sources and grid-connected systems, the PV array can connect to the grid and fulfill grid code requirements with less complexity. The DC voltage from the PV array is frequently altered to an AC voltage using a power electronic voltage source converter (VSC).

Voltage in transmission and distribution has been managed over time by the use of active and reactive power. Voltage regulation is the process of controlling the difference in voltage between two endpoints, such as transmission and distribution. Together, static synchronous compensators (STATCOM) and static variable compensators (SVC) ensure that the voltage across the load stays within acceptable bounds. Impedance creates problems with voltage regulation, leading to either overvoltage or voltage drops below normal under heavy load conditions.

A power electronic interface between the source and the load is suggested to enable output voltage management [2] while also improving power quality (PQ) to address the voltage imbalance. The recommended method is distinctive in that it uses a multilevel inverter to offer a dual benefit. The term "multilevel" comes from the three-level converters. To achieve high output voltage levels, the semiconductor switches' commutation combines several direct current (DC) sources. The benefits of multilevel inverters include better PQ, more electromagnetic compatibility, reduced switch losses, and enhanced voltage capacity. The three architectures of multilevel inverters are neutral fixed or diode fixed multilevel inverters, flying capacitor multilevel inverters, and cascaded multilevel inverters (CMLI). This study makes use of the CMLI.

The main purpose of CMLI [2] is to combine numerous dc sources, such as batteries or solar cells, to provide the necessary voltage. If the H-bridge DC-link voltages are equivalent, the CMLI is said to be asymmetrical. Because solar PV voltages might change depending on the climate, asymmetrical inverters are strongly advised. Varying asymmetrical inverters have different dc-link voltages [4][5]. The design of the PV controller, the inverter, the interface, and the scheduling of microgrids [6][7] all play significant roles in enhancing the performance of grid-connected PV systems. Energy trading in microgrids is improved by the application of various learning algorithms [8].

Consumers increasingly use microgrids, which employ renewable and alternative energy technologies, to satisfy their energy demands and lessen environmental issues. Utilizing these more recent technologies through a microgrid significantly improves resource efficiency, PQ, and the availability of dependable electricity. Grids that are zone-based or dispersed now incorporate these more contemporary elements as a result of recent grid developments like multi-microgrids, interconnected alternating current (AC-AC), and AC-DC microgrids.

According to IEEE 519 standards, the maximum individual harmonic component percentage for electrical systems with a voltage of 69 kV or less is 3 %, and the maximum total harmonic distortion is

5 %. The standard establishes aims for the plan of electrical systems with both linear and non-linear loads, point of common coupling, and total harmonic distortion should be less than 3 %.

This manuscript is organized as follows: The literature review is explained in section I. The PV system was modeled, and its performance was examined in section II. Cascade MLI design, its performance analysis, and grid-connected PV system controllers' design, performance analysis, and comparisons are explored in section III, and the manuscript is concluded in section IV.

Md. Halim Mondol *et al.* [9] used the half-height neutral clamped (HHNPC) inverter, a new 1- ϕ MLI with fewer switches. The suggested MLI comprises a 10 kW PV system as a DC source, switching devices, & a reduced number of control diodes compared to traditional topologies. Unipolar variation is used to create the triggering points for the recommended inverter, which results in the lowest THD in both production voltage & current. The suggested inverter architecture is modeled as a 1- ϕ , nine-level inverter. The technology is modeled using MATLAB/Simulink. Additionally, the recommended and traditional topologies are contrasted.

N. Thombre *et al.* [10] have suggested and published a variety of unique CMLI topologies in the literature. The primary drawback of the three-phase CMLI implementation is the high cost of power semiconductor components and the input dc supply necessary for all suggested topologies. This article offers a fresh, expanded concept for reducing the quantity of dc power supply, control switches, and diodes in an existing CMLI design. The new optimal models include two phases: a flow phase that may be changed to incorporate a current flow topology, and a phase generator stage that comprises a typical 3- ϕ 2-level inverter (CTPTLI) and three bidirectional switches. The predicted topologies are validated by extensive modeling analysis. The findings may be used to show how the proposed technique can decrease the device numbers in the current topologies while preserving their concerted operation.

A novel CMLI architecture that drastically decreases the number of control switches and DC voltage sources were presented by N. Thombre *et al.* [10]. The proposed system employs an asymmetrical MLI with 11 unidirectional switches, three diodes, and four direct current voltage sources to provide 21 levels of output. The benefit of this topology is that it reduces the number of switches, gate driver circuits, and DC sources, all of which are now two (2 no.). Without compromising the inverter's superior output, it also lowers the hardware's charge, difficulty, & space necessities.

For the cascaded switched diode multilevel inverter, C.K. Kishore *et al.* [11] and his colleagues proposed a sinusoidal pulse width modulation (SPWM) control method as opposed to clock phase shifting (CSDMLI). Two similar resistive loads are associated with the CSDMLI. The proposed MLI reduced the harmonic level by up to 12.76 % by delivering many loads when related to the previous control method, which produced a 16.82 %

harmonic bias. To switch between loads, a basic pulse-width modulation approach is used. In high-power medium voltage applications, MLIs are also used.

On the control switches, Hosseinzadeh *et al.* [12] found lower upright voltage and lower harmonics. The fact that multilayer inverters need a lot of switching components makes control challenging, which is a major drawback [12]. The design and construction of an unconventional switch-diode MLI for CMLI are discussed in this study. With fewer control switches, DC sources, and a lower overall obstructive voltage on the switches, the intended irregular MLI yields 31 levels. In order to verify the benefits and limitations of MLI, the suggested topology is connected to the present CMLI.

A brand-new two-stage CSDMLI design for medium-voltage alternative energy integration has been created by L. Way *et al.* [13]. The reduction of switches and gate drivers in MLI is the main goal of this design. The PQ of a grid-connected system was enhanced by Narasimhulu *et al.* [14] using a variety of intelligent controllers for cascaded H-bridge MLI and shunt active power filter applications. For effective planning and seamless operations, Farooqi *et al.* [15] have concentrated on several connectivity configurations of dispersed generating penetration. Renewables are incorporated into modern systems to maintain a balance between supply and demand and to support clean energy projects. The learning strategy for microgrid reconnection has been

described by C. Lassetter *et al.* [16]. The performance analysis of a multilayer cascade H-bridge-based active power filter under load change was described by Narasimhulu *et al.* [17]. Hui-Qiong Deng *et al.* [18] discussed the safety and economics of the preventative control technique for cascading failures. State of charging (SoC) balancing techniques for power matching in cascaded H-bridge MLI have been described by J. Yu *et al.* [19].

This research suggests several artificial intelligence control methods for the CMLI to enhance the voltage level in cascaded H-bridge MLI to enhance the quality of power under various loading scenarios. The THD, active power, and power factors for several control algorithms are compared in this work. These cutting-edge network topologies may maximize the usage of renewable and substitute energy sources. Linking two or more microgrids, for instance, enables standby allocation, voltage, and frequency support and ultimately increases the reliability and flexibility of the linked microgrids overall.

Figure 1 displays the whole block diagram for PQ control of a grid-connected PV system. To extract most of the power from the system, a 10 kWp PV system with a boost converter and a cascaded feedforward neural network-based MPPT Control algorithm is used. A set of 4 such PV systems are then used to convert DC to AC using a 9-level cascaded multilevel inverter, allowing the system to be integrated with the grid. The grid and load

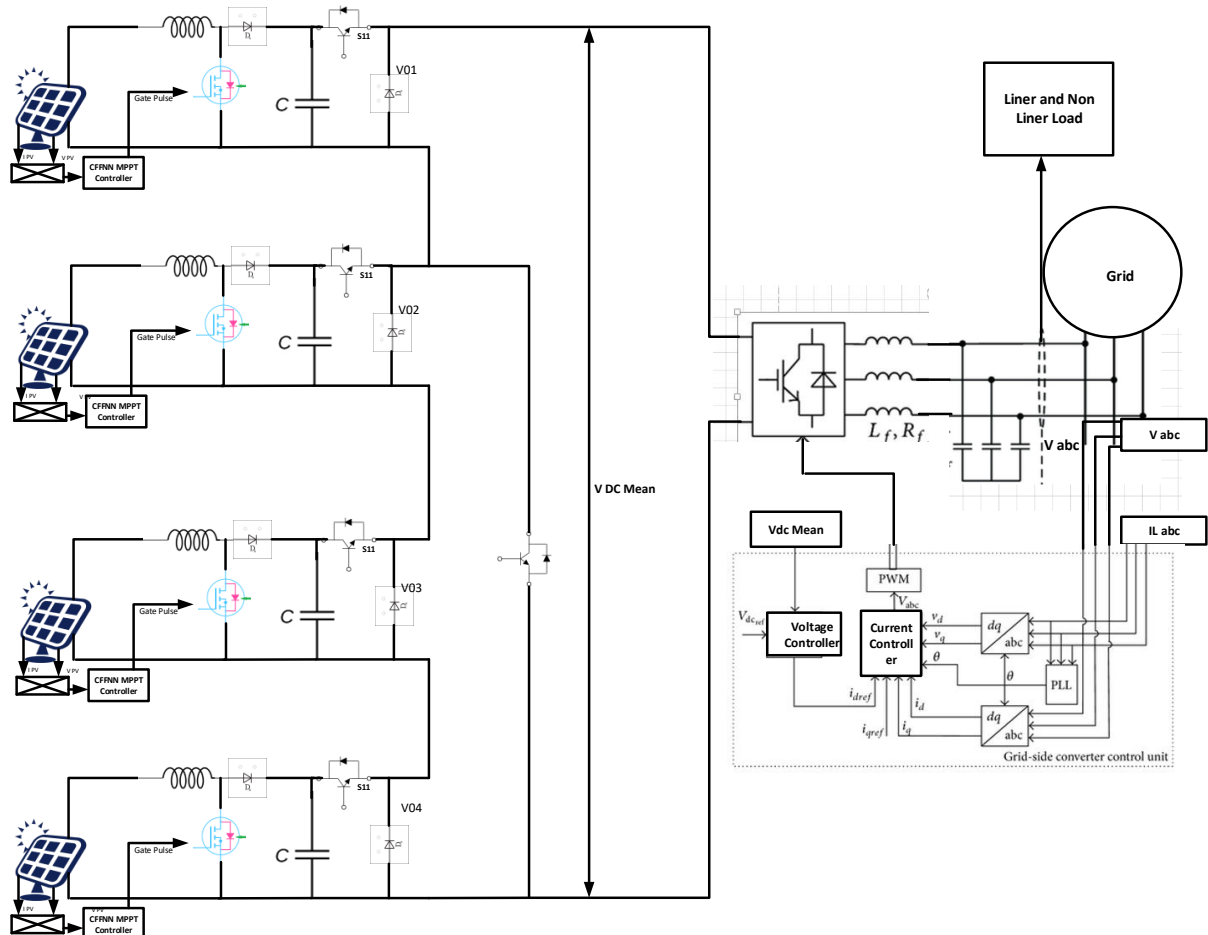


Figure 1. Complete block diagram of PQ control of grid-connected PV system

voltages are used as a reference to create the firing pulses for the cascaded multilevel inverter employing multiple controllers in the feedback system.

PV systems may have several detrimental effects on the grid if PV penetration is very high. Reverse power flow, overvoltage throughout the distribution system, trouble in controlling voltage, phase imbalance, PQ issues, enhanced reactive power, and difficulty detecting islanding are among them.

This work is intended to:

- Studying a PQ improvement in a grid-connected PV system using voltage and current controller topologies.
- Train the novel deep neural network (DNN) using input parameters, including grid power changes, switching pulses, and the proportional plus integral (PI) controller's target gain settings. During the testing period, the DNN predicts the PI controller's gain parameters based on grid side parameter fluctuation, and the grid side's PQ has been improved.
- Evaluate the performance of the DNN control technique under various operating conditions [20] with PI, Fuzzy, ANFIS, and cascaded feedforward neural network (CFNN) Controllers.

II. Materials and Methods

A. Modeling of PV system

In Figure 2, an additional series and parallel resistors link the solar cell to a diode as a dependent current source. It's important to note that when solar light is not present, no power is produced, and the PV cell behaves like a diode [21]. The amount of sunlight that strikes the PV cell (photo-current) regulates the real current coming from the PV cell (Figure 2). Equation (1) illustrates how the voltage loss across the diode will impact the voltage generation in the PV cells.

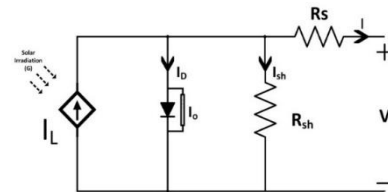


Figure 2. The equivalent PV cell circuit

$$V = \left(\frac{NKT}{Q} \right) \ln \frac{I_L - I_o}{I_o} + 1 \tag{1}$$

The generated current by light (radiation) is shown in equation (2)

$$I_L = \left(\frac{G}{G_{ref}} \right) * (I_{L\ ref} + \alpha_{Isc} (T_C - T_{C\ ref})) \tag{2}$$

Reverse saturation current is shown in equations (3) and (4)

$$I_o = I_{or} \left(\frac{T_c}{T_{ref}} \right)^3 e^{\frac{(Q+Eg)}{(K+N) \left(\frac{1}{T_{ref}} \right) - \left(\frac{1}{T_c} \right)}}$$
(3)

$$I_{or} = \frac{I_{scn}}{e^{\left(\frac{V_{ocn}}{N+V_{tn}} \right)}}$$
(4)

Current S C ($I_{sh} = I_L$) as shown in equation (5)

$$I_{sh} = (I_L - I_o) * \left(e^{\frac{eV}{kT}} - 1 \right) A \tag{5}$$

B. Grid integration of PV systems and design simulation of MLI

The CMLI is well known for grid interconnection of alternative energy sources to improve system PQ and reliability. The suggested CMLI was designed using a small number of power electronics (PE) switches to decrease THD for both the current and voltage waveforms. Here, five metal oxide semiconductor field-effect transistor (MOSFET) PE switches are engaged, with 4 PV models coupled to each PE switch, as illustrated in Figure 3. The suggested multilevel inverter uses the staircase modulation technique to generate pulses. The

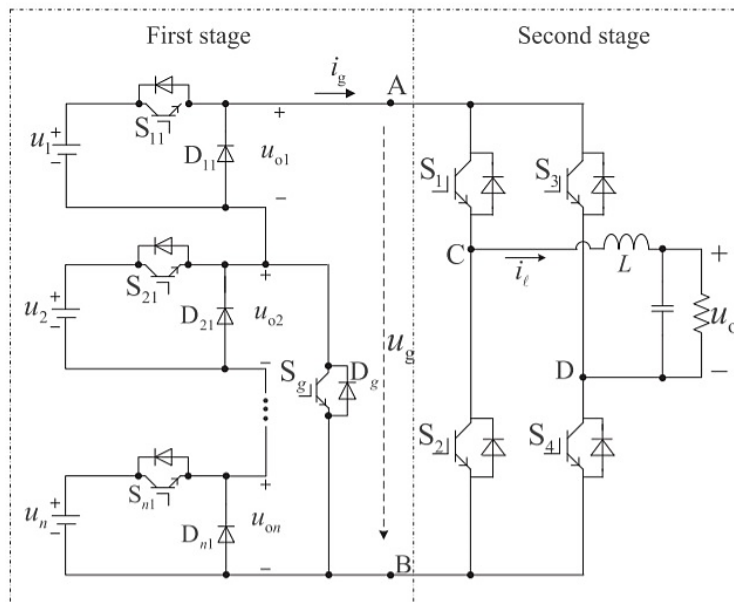


Figure 3. CMLI architecture (9-level) for a PV system linked to the grid

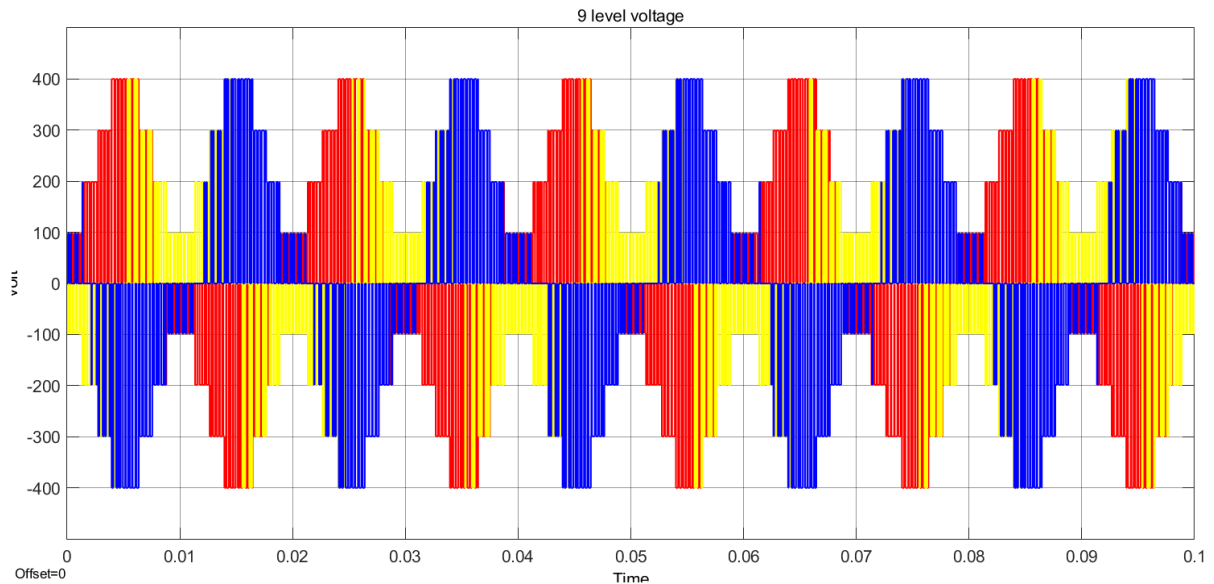


Figure 4. The waveform of the multi-level inverter output voltage with 3 phases and 9 levels

suggested MLI was designed in two phases, DC-DC and DC-AC, utilizing an H-bridge. The 3-phase output voltage is shown in Figure 4.

C. Modeling of microgrid-connected PV system

The simulation model grid integration of PV systems with an MLI and proposed controllers, VSC for bridged inverter, voltage control loop in with PI controller in VSC, and a proposed current controller to regulate the current in VSC with various intelligent controllers were shown in Figure 5, Figure 6, Figure 7, and Figure 8 respectively. To overcome the above time lag problem, the proposed DNN controller is implemented in the MATLAB/Simulink tool for standalone and grid-connected modes of operations, and the same

algorithm is compared with connecting CFNN, ANFIS, Fuzzy, and PI controller algorithms to show that the proposed algorithm gives better response with non-linear and unbalanced loading conditions.

D. Cascaded feed forward neural network controller

The most fundamental element of a neural network is a neuron (NN). Synaptic weight serves as the link between neurons. Figure 9 depicts this NN's five invisible levels and production layer. A CFNN is one such type of NN which architecture is shown in Figure 10. The information process in CFNNs is conveyed from the contribution nodes to the hidden nodes and from the hidden nodes to the output nodes. The initial connection for each layer in the

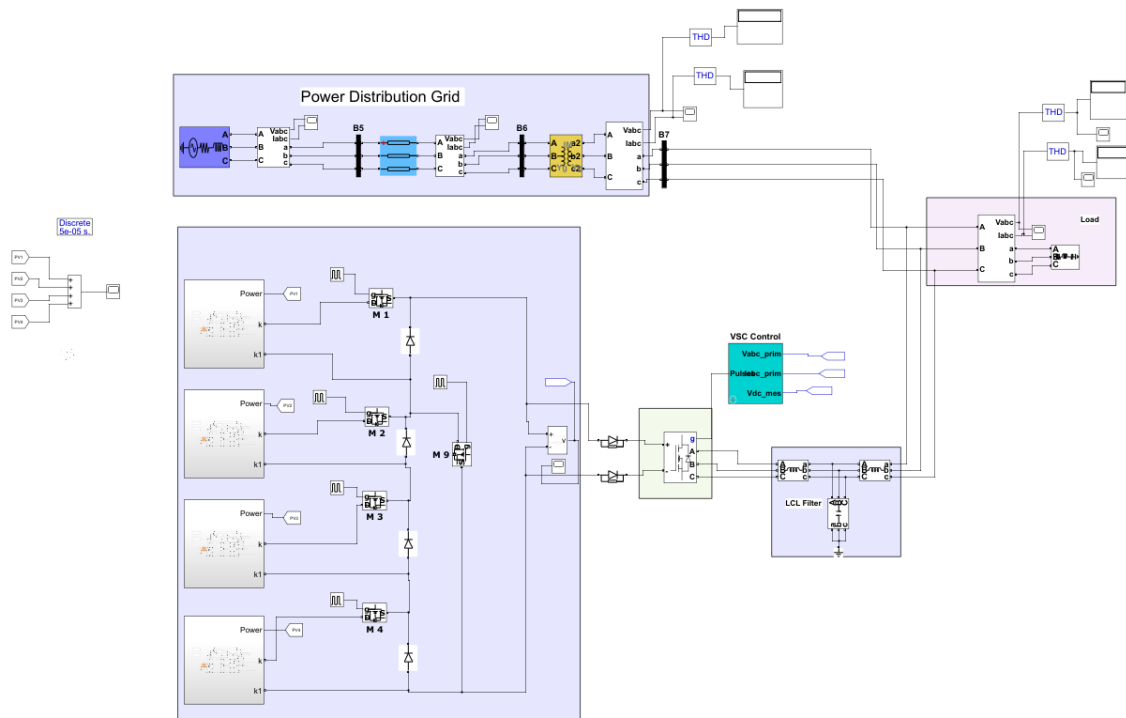


Figure 5. Photovoltaic systems integration into micro-grid simulation model using a proposed controller and multilevel inverter

VSC Main Controller

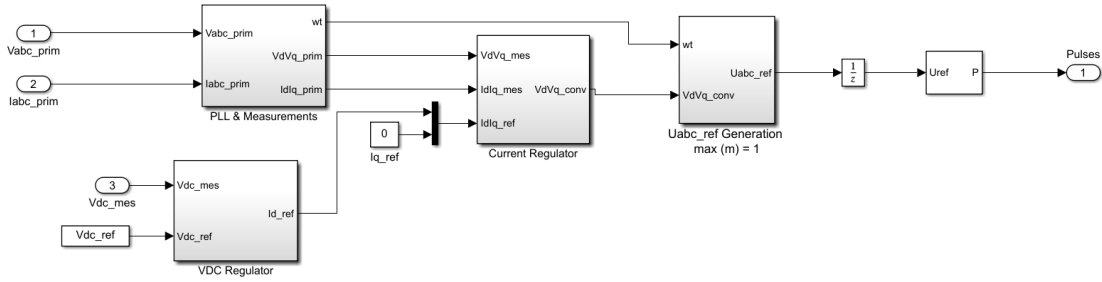


Figure 6. VSC regulator for photovoltaic systems integration with microgrid

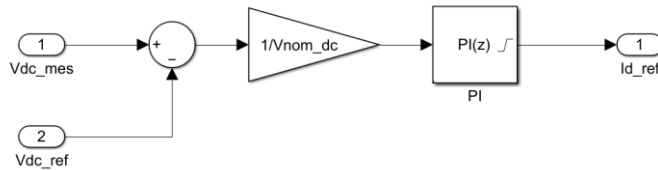


Figure 7. Photovoltaic system micro-grid connectivity using VSC

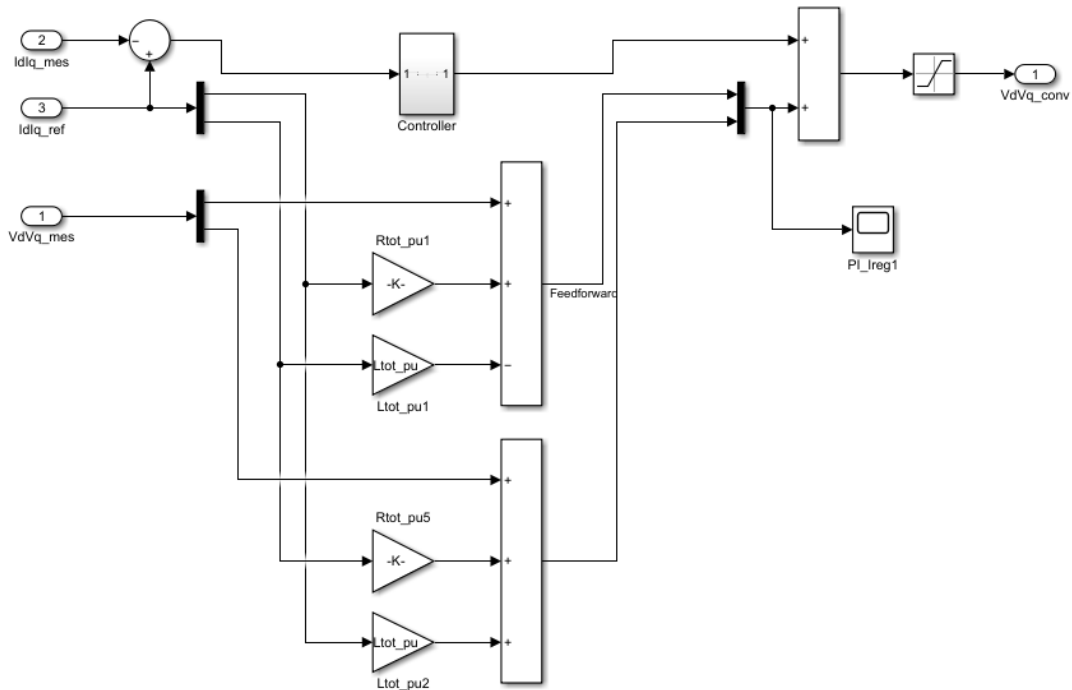


Figure 8. Suggested micro-grid interconnection of a photovoltaic system with current regulator controller

network goes from the input to that layer, and the next link travels from that layer to the following levels.

In a perceptron, the relationship between the input and the output is direct. However, a CFFNN has an indirect connection between input and output. The unseen layer's relationship is both linear and non-linear in shape because of a stimulation function. It is feasible to build a network that connects the input and output layers by combining perceptron and multilayer networks. The CFFNN produced by this connection architecture is called cascade forward. One option for the CFFNN model is in equation (6).

$$y = \sum_{i=1}^n f^i w_i^i x^i + f^o (\sum_{j=1}^k w_j^o f_j^h (\sum_{i=1}^n w_{ji}^h x_i)) \quad (6)$$

where f_o is the activation function on the output layer, f_j^h is an activation function on the hidden layer, w_j^o is the weight of the j th neuron at the output layer, w_{ji}^h is the weight of the j th neuron at the hidden layer, and w_i^i is the weight of the i th neuron at the input layer

The job in issue is the stimulation task between the contribution and production layers, and the stimulation function from the contribution layer to the production layer is represented by the weight in the contribution layer's stimulation function. equation (6) changes to resemble equation (7) when an additional bias is applied to the contribution layer and each neuron in the hidden layer has an activation function of fh.

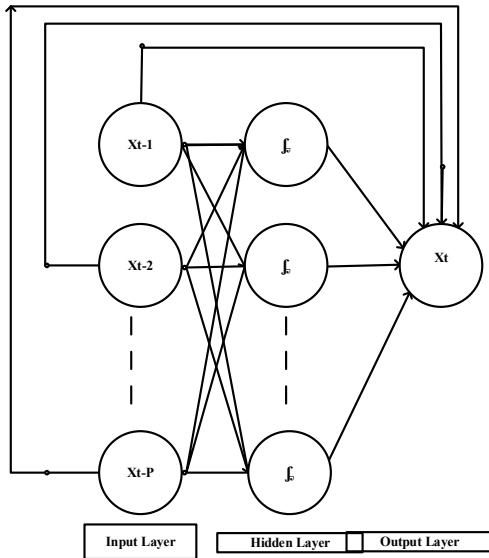


Figure 9. CFFNN architecture – five layers

$$y = \sum_{i=1}^n f^i w_i^j x_i + f^o \left(w^b + \sum_{j=1}^k w_j^o f_j^h \left(\sum_{i=1}^n w_{ji}^h x_i \right) \right) \quad (7)$$

where ω^b is the weight of the bias from the input.

The CFNN model often employs time series data. The outcome is present data at X_t level because neurons in the input layer delay the time series data represented by the data at X_{t-1} , X_{t-2} , X_{t-3} , and X_{t-p} levels. To increase the size of the entire network by the number of neurons in the contribution layer, the network weight must be computed and modified. The feedforward algorithm on CFNN, known as backpropagation, consists of three stages: initial weight computation, pattern error counting, and further weight calculation. The error is computed during the feedforward phase, and then the development continues with the feedforward design (the variation in the result to the target). The next step is to adjust the weights before rerunning the computation to make sure everything is still accurate. As long as no error or iteration halt is found, the process is resumed. This section briefly discusses the conjugate gradient optimization method for modifying the CFNN's weights. Assume that is a length- s weight vector and that the goal is

to locate all network weights as indicated by equation (8).

$$e = \frac{1}{2} (X_t - \hat{X}_t)^2 \quad (8)$$

The optimistic positive matrix dimension is s^*s

Whereas $QT = Q$ is defined as Q . The following are the stages of the Conjugate Gradient Optimization procedure:

Step 1: Set $k = 0$ & choose the starting position as 0

Step 2: Determine the gradient of the initial weight as shown in equation (9)

$$g^{(0)} = \frac{de}{dw^0} = \frac{de}{dw|_{w=w^0}} = \left[\frac{de}{dw_1^{(0)}} \dots \dots \frac{de}{dw_s^{(0)}} \right]^T \quad (9)$$

If $g^{(0)} = 0$ then stop and then obtained the optimal weight $\omega^{(0)}$. Else, $d^{(0)} = g^{(0)}$

Step 3: Determine α_k using equation (10)

$$\alpha_k = \arg \min_{\alpha \geq 0} e(w^{(k)} + \alpha d^k) = - \frac{g^{(k)T} d^{(k)}}{d^{(k)T} Q d^{(k)}} \quad (10)$$

Step 4: Determine $\Omega^{(k+1)}$ using equation (11)

$$\Omega^{(k+1)} = \Omega^k + \alpha_k d^{(k)} \quad (11)$$

Step 5: $g^{(k+1)} = \frac{\partial e}{\partial w^{(k+1)}}$ if $g^{(k+1)} = 0$ stop and the optimal weight is $w^{(k+1)}$

Step 6: Determine β_k using equation (12)

$$\beta_k = \frac{g^{(k+1)T} Q d^k}{d^{(k)T} Q d^k} \quad (12)$$

Step 7: Determine $d^{(k+1)}$ using equation (13)

$$d^{(k+1)} = -g^{(k+1)} + \alpha_k d^{(k)} \quad (13)$$

Step 8: $k = k+1$: drive to stage 3

Epoch repetition is also referred to as weight searching on CFNN in feedforward neural networks (FFNN). To start the repetition method, the program must not have satisfied the iteration termination condition before epoch $k = K$. The direction vector is reset after each iteration because this method can't guarantee convergence in the n steps, and the procedure is continued until the termination condition is met. In the non-linear model, Q is a non-constant Hessian matrix that is produced for each

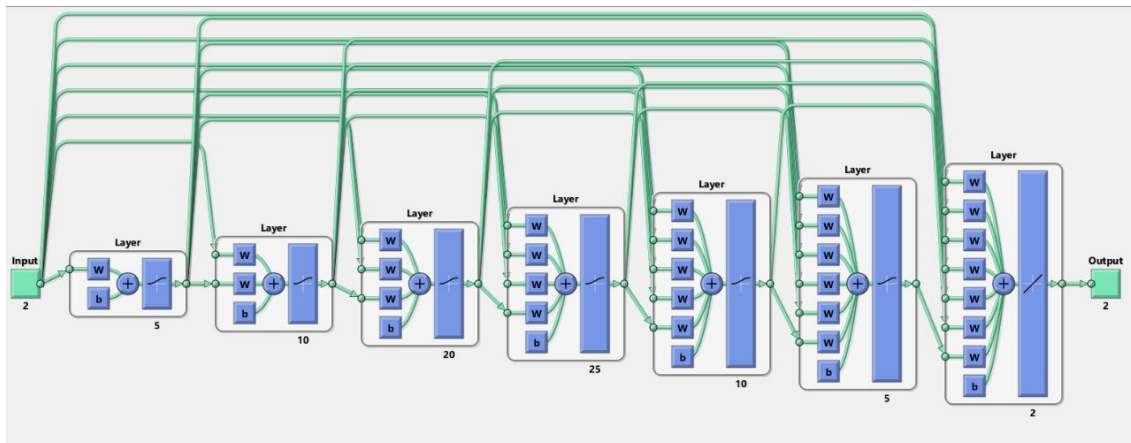


Figure 10. The architecture of CFFNN

iteration. An algorithm for eliminating Q is employed to make the method straightforward, with the only sources of algorithm reliance being the function and gradient value for each iteration. One of the many formulae for substituting $Qd(k)$ with other forms is the Hestenes-Stiefel formula, or $Qd(k)$. Thus, the k may be expressed as in equation (14).

$$\beta_k = \frac{g^{(k+1)T}[g^{(k+1)}-g^k]}{d^{(k)T}[g^{(k+1)}-g^k]} \tag{14}$$

The best validation performance of CFFNN model is shown in Figure 11, and the best-validated performance is at the 25th epoch with 7.3503e-08 mse. Figure 12 shows the gradient, Mu, and validation checks with CFFNN's controller at epoch

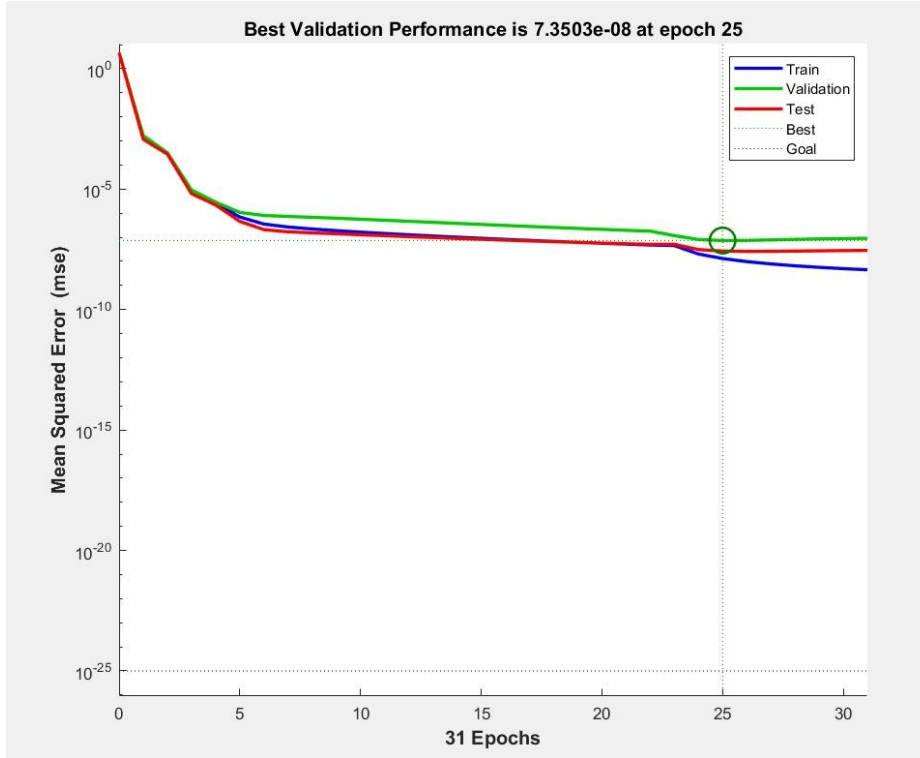


Figure 11. The validation performance of the CFFNN model (7.3503e-8 at epoch 25)

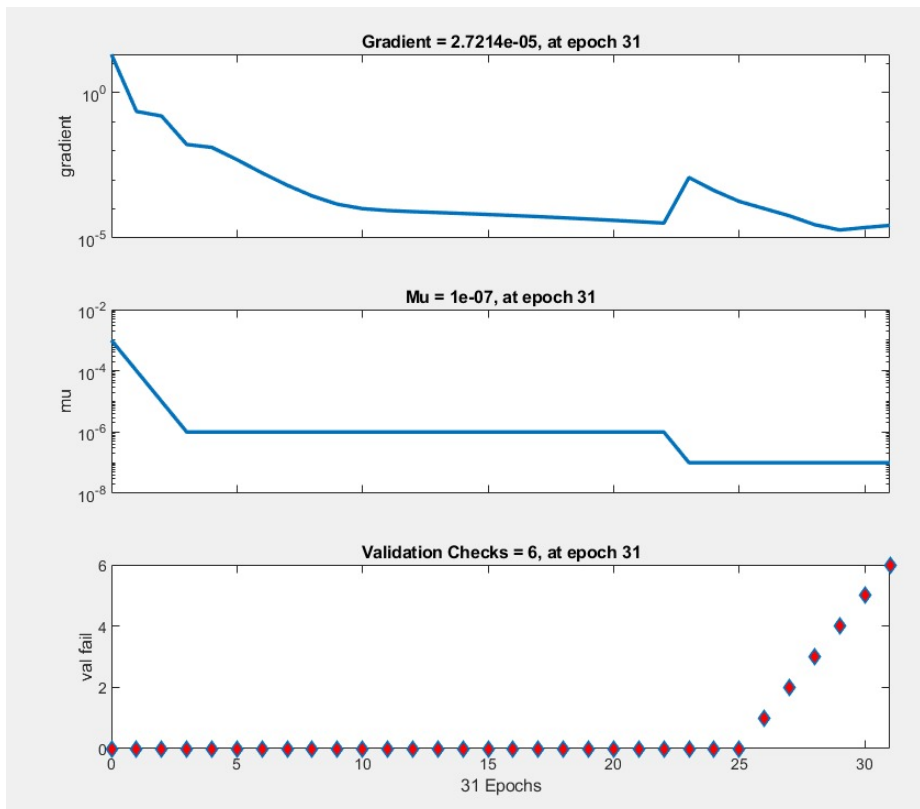


Figure 12. Gradient, Mu, and validation checks with CFFNN controller

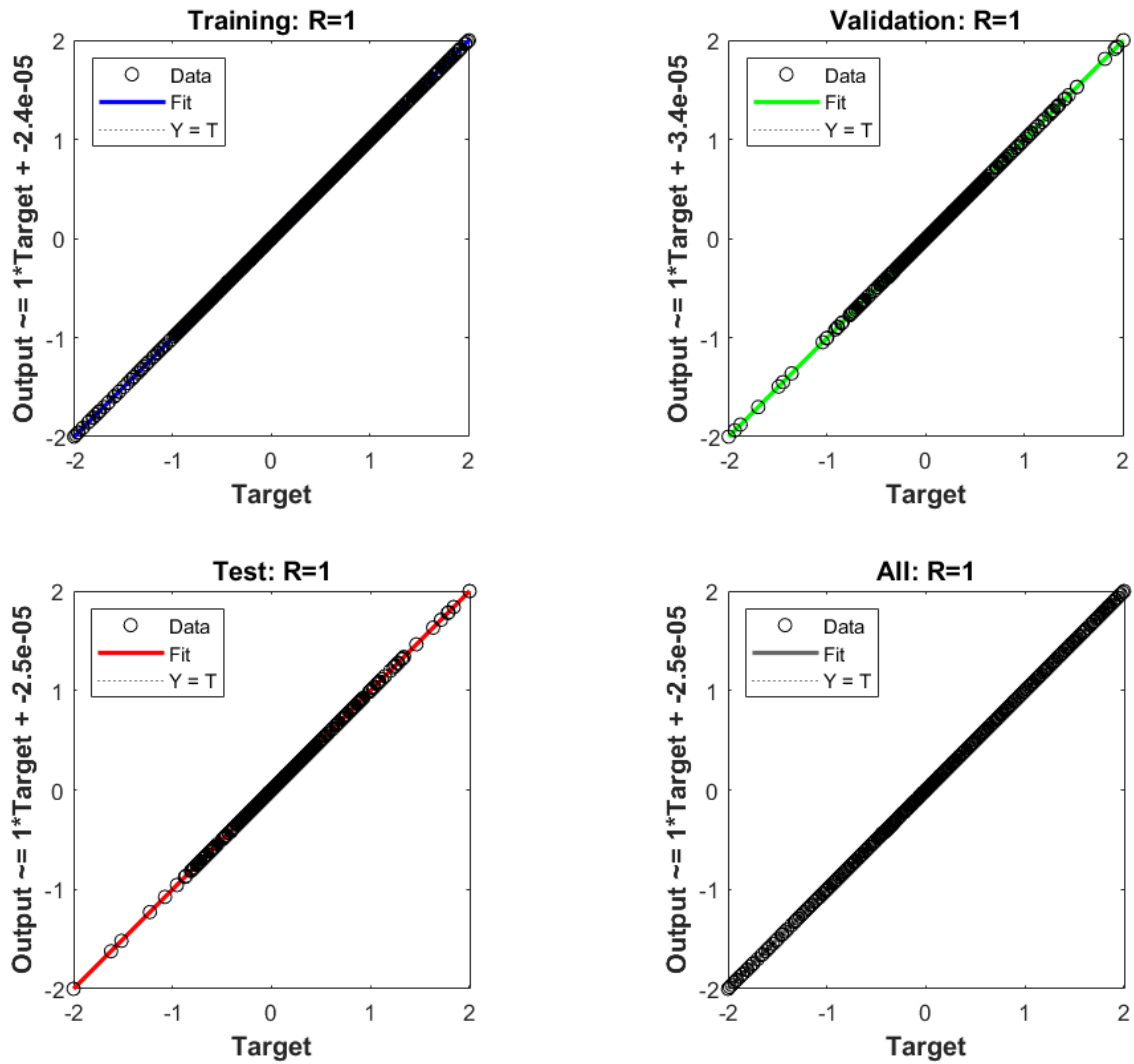


Figure 13. Training, validation test, and regression performance with CFFNN controller

31. In Addition, the training, the validation test, and the regression performance with CFFNN controller are shown in [Figure 13](#).

E. Deep neural network (DNN)

Basic connected components known as neurons make up an artificial neural network (ANN). Each neuron is a mapping with many inputs and a single output. The output of a neuron is inversely correlated with the sum of its inputs. A neuron is produced by an activation function, which is a function. Since a single neuron's single output can be used as an input to other neurons, the symbol for a single neuron shows the number of arrows emanating from the neuron. The input and output layers of the perceptron's two-layer network are the sole layers.

The perceptron is the source of the signal. The signal is directly transferred from the contribution layer to the production layer in a perceptron. Production and contribution are inversely correlated. Transferring weighted amounts from donations to production implies a close relationship between the

two levels. Because the NN contains many layers between input and output, it is known as a "multilayer perceptron". The multilayer perceptron system is also recognized as an FFNN in NN modeling. The FFNN network has an additional layer called the hidden layer. The signal is guided in a weighted fashion from the input layer to the unseen layer.

The contribution signals are received by the buried layer, which then distributes them to the neurons. The initiation function of the layer then progresses signals that arrive at the neurons of the unseen layer. The initiation function of the unseen layer is a non-linear function that may be utilized as a transfer function. In the unseen layer, the weighted total of the respective neuron's output is then transmitted to the output layer. Before being transmitted to the output layer, the incoming signal is processed by this layer's activation function. Identity mapping is a common activation function for the production layer, as it assures that the productivity made in this layer is equal to the contribution signal. The MLP with n contributions x_i ,

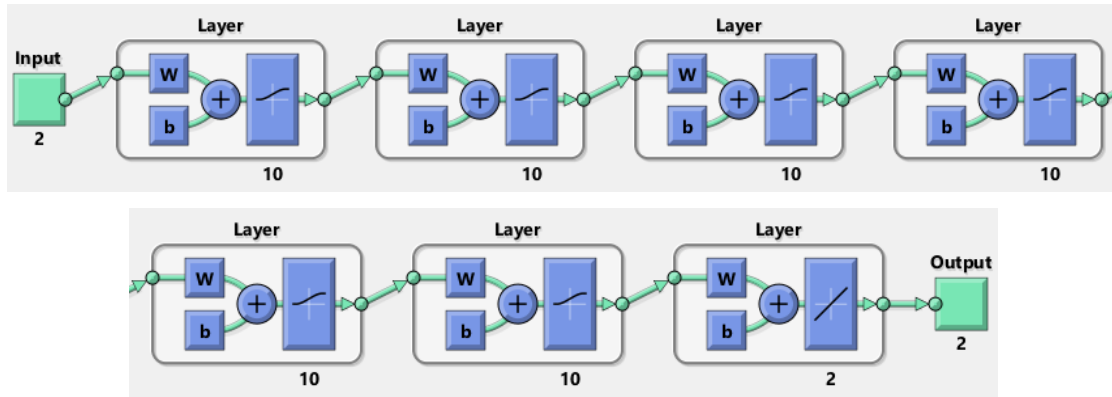


Figure 14. The architecture of DNN

where $l = 1, \dots, n$, one production neuron y and k unseen neurons layer are shown in Figure 14.

The output of a suppressed layer neuron is denoted by z_j , where $j=1, \dots, k$. The contribution x_1, \dots, x_n is circulated to the neurons by the unseen layer. The initiation function of the respective neuron in the contribution layer is called uniqueness mapping. A neuron's initiation function in the unseen layer is signified as "fh" whereas a neuron's initiation function in the production layer is written as "fo". The initiation functions are all R to R. Figure 14 shows the deep neural network architecture, and the same can be expressed in a mathematical equation as shown in equation (15)

$$y = f^o \left(\sum_{j=1}^k w_j^o f_j^h \left(\sum_{i=1}^n w_{ji}^h x_i \right) \right) \quad (15)$$

where f^o is the production layer initiation function, and f_j^h is the unseen layer initiation function, the preceding Equation becomes fh if a bias is applied to the contribution layer and the initiation function of the respective neuron in the unseen layer is fh, as shown in equation (16)

$$y = f^o \left(w^b + \sum_{j=1}^k w_j^o f_j^h \left(\sum_{i=1}^n w_{ji}^h x_i \right) \right) \quad (16)$$

where the bias to production weight is w^b , while the bias to unseen layer weight is w_j^b .

Figure 15 shows the best validation of the DNN model (9.9565e-11 at epoch 2703). Figure 16 shows gradient, Mu, and validation checks with DNN's controller. Moreover, Figure 17 shows the training, validation, testing, and overall performance with DNN's controller.

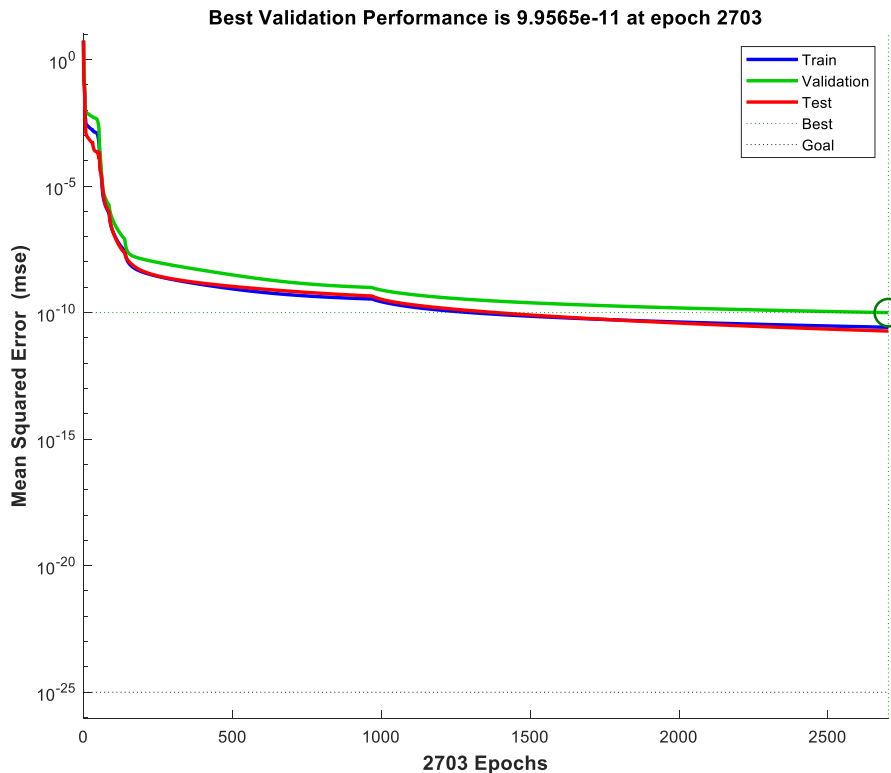


Figure 15. The best validation of the DNN model (9.9565e-11 at epoch 2703)

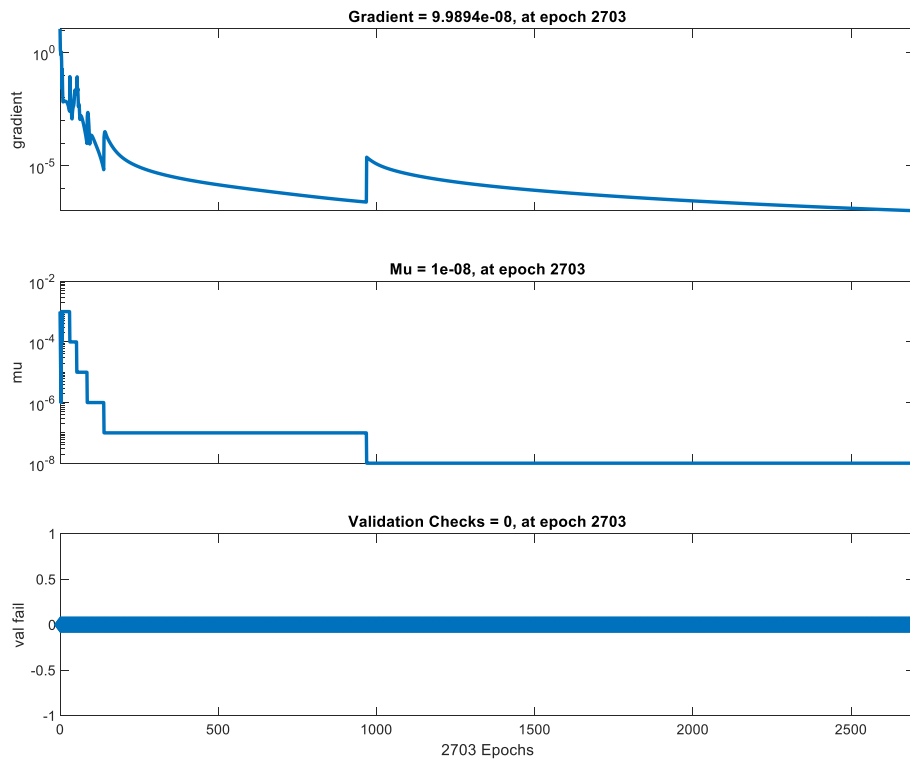


Figure 16. Gradient, Mu, and validation checks with DNN Controller

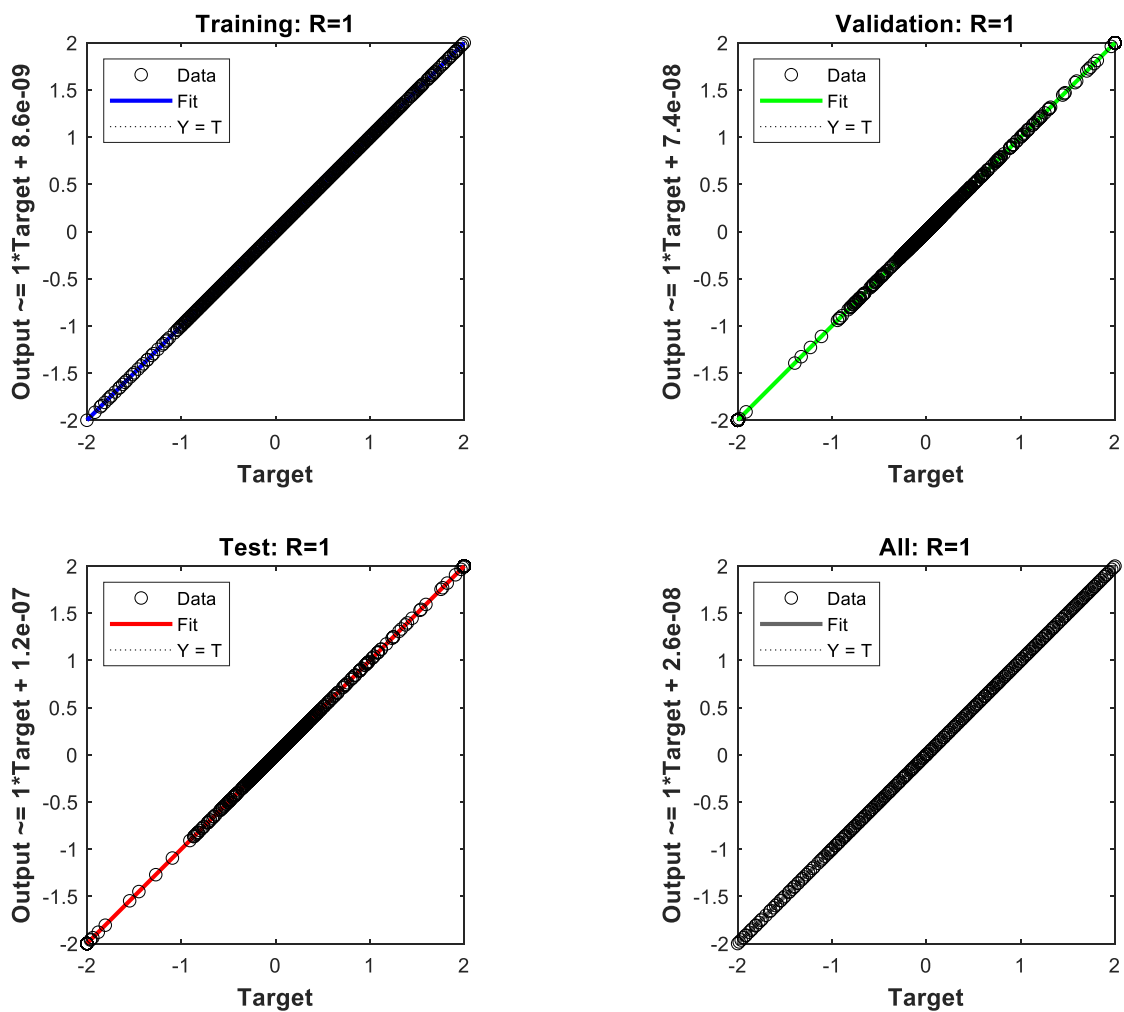


Figure 17. Training, validation, testing, and overall performance with DNN controller

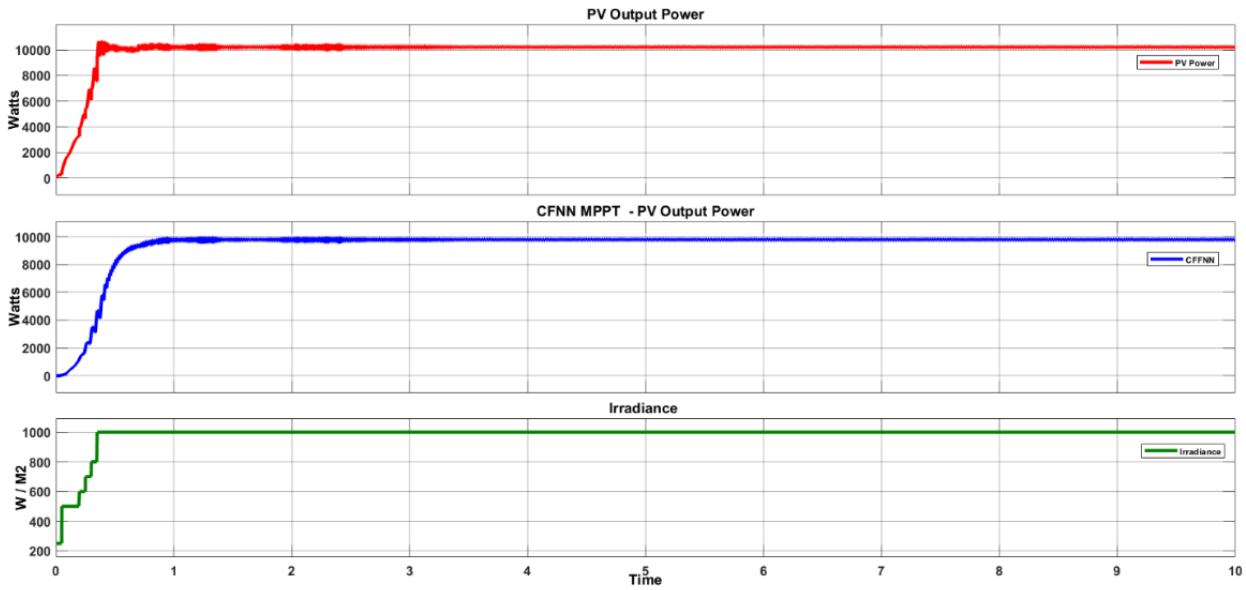


Figure 18. The output power of 10 kW PV system with CFFNN MPPT controller

III. Results and Discussions

Figure 18 shows the 10 kWp PV system output power and PV-connected boost converter output power with cascaded feedforward neural network MPPT algorithm, with variable irradiance.

Figure 19 shows the 10 kWp connected boost converter output voltage and current. From the figures, it is clear that the efficiency of the 10 kW PV system is maintained at 99.9%, and the boost converter with CFFNN MPPT algorithm output voltage is around 500 Volts.

A. CFFNN controller for standalone system

In a Matlab environment, the suggested CFFNN-based MPPT technique was established. More than

90,000 data points are employed to offer training (80 %), testing (10 %), and validation (10 %).

The suggested system's best validation performance is highlighted at $7.3503e-8$ at epoch 25, as shown in Figure 10. As previously shown in Figure 11, many parameters were utilized at epoch 31 to explore the best validation performance of current regulation, including gradient $2.7214e-5$ and $\mu 1e-7$.

Figure 20 demonstrate the overall performance of the suggested current regulator (load voltage, load current, active, reactive powers, and power factors) using the CFFNN algorithm for a standalone system. The power factor by using CFFNN based controller for a standalone system is 0.996 which is almost unity as shown in Figure 20(e).

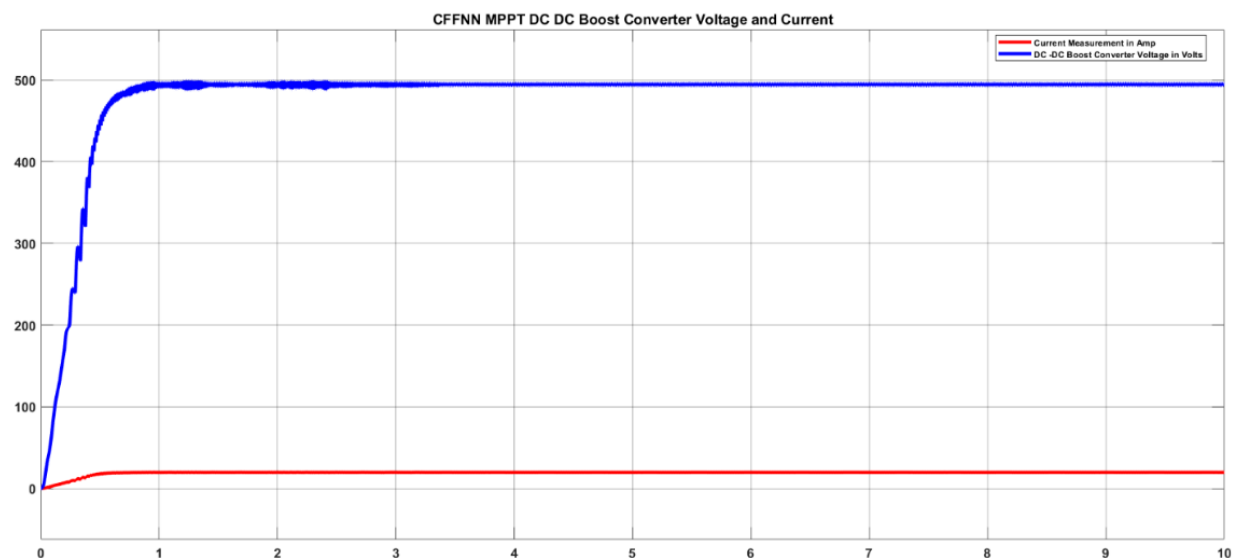


Figure 19. Boost converter output voltage and current with CFFNN MPPT controller

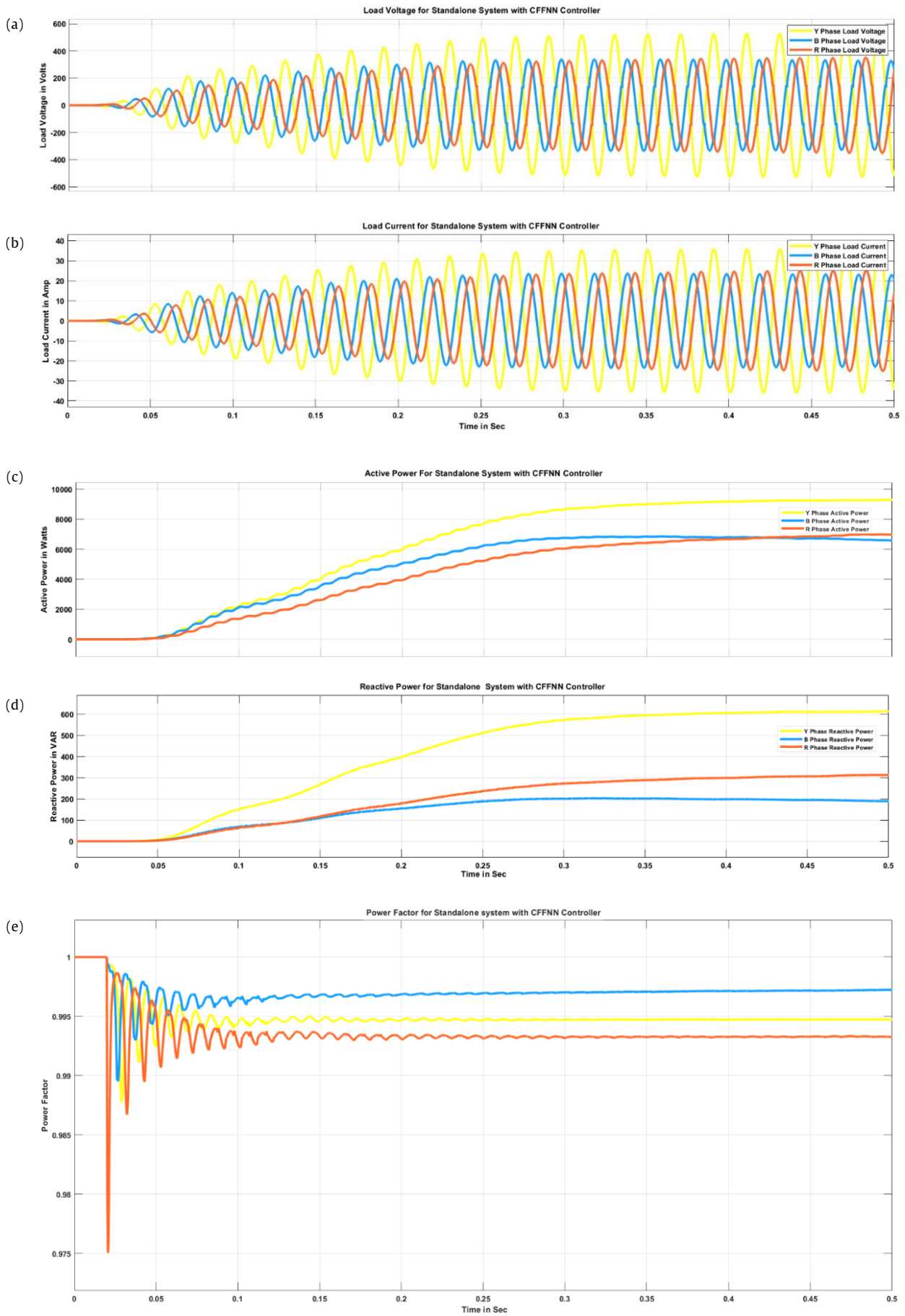


Figure 20. Three-phase load waveform of CFFNN controller for a standalone system: (a) load voltage; (b) load current; (c) active power; (d) reactive power; and (e) power factor

Figure 21 and Figure 22 give the total harmonic distortion of load voltage and load current at different loading conditions like unbalanced and non-linear load for a standalone system in a

specified time period with CFFNN current controller. From the figure, it is clear that the THD for load voltage is 3.59 %, and the load current is 1.16 %.

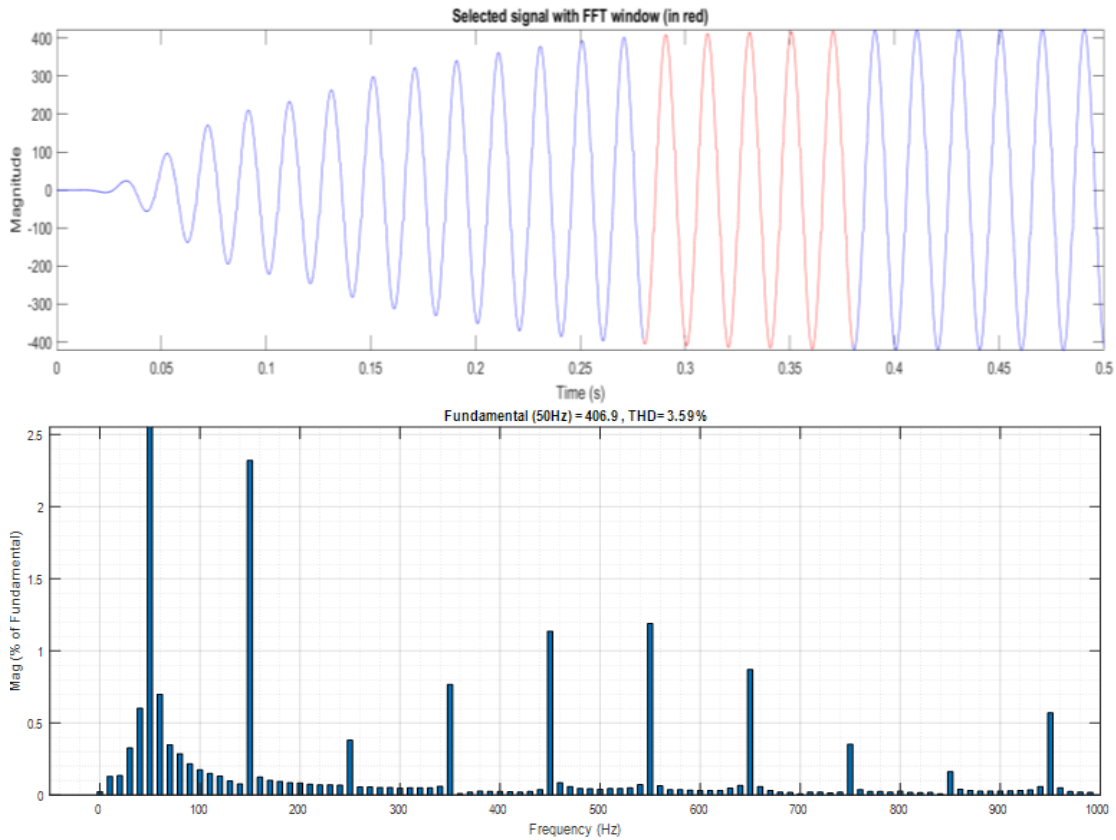


Figure 21. Load voltage THD for a standalone system with CFFNN controller

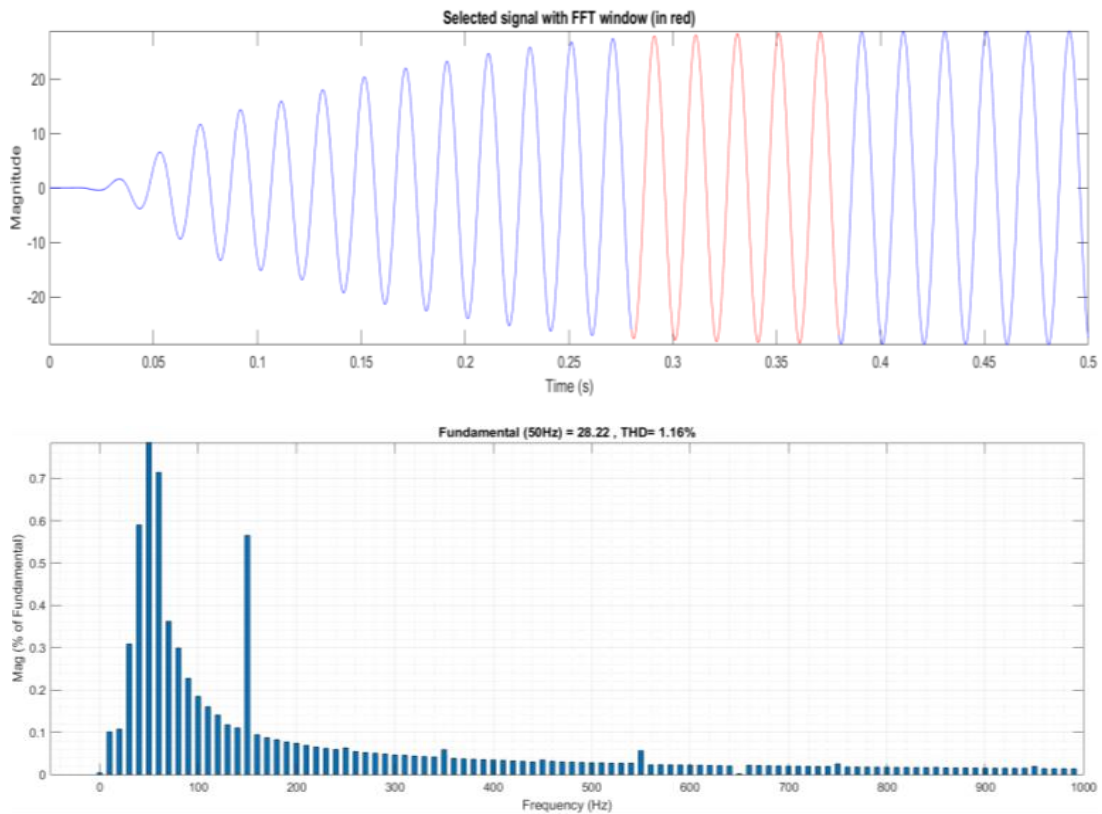


Figure 22. Load current THD for a standalone system with CFFNN controller

B. CFFNN controller for grid integrated PV system

Figure 12 and Figure 13 present the results of an evaluation of the recommended current regulator algorithms' overall performance utilizing parameters, training, testing, and validation. The created current

controller algorithm has been applied in the planned CMLI for coordinating into the grid, and the grid-connected model's load voltage, current, active power, reactive power, and power factor are analysed in Figure 23.

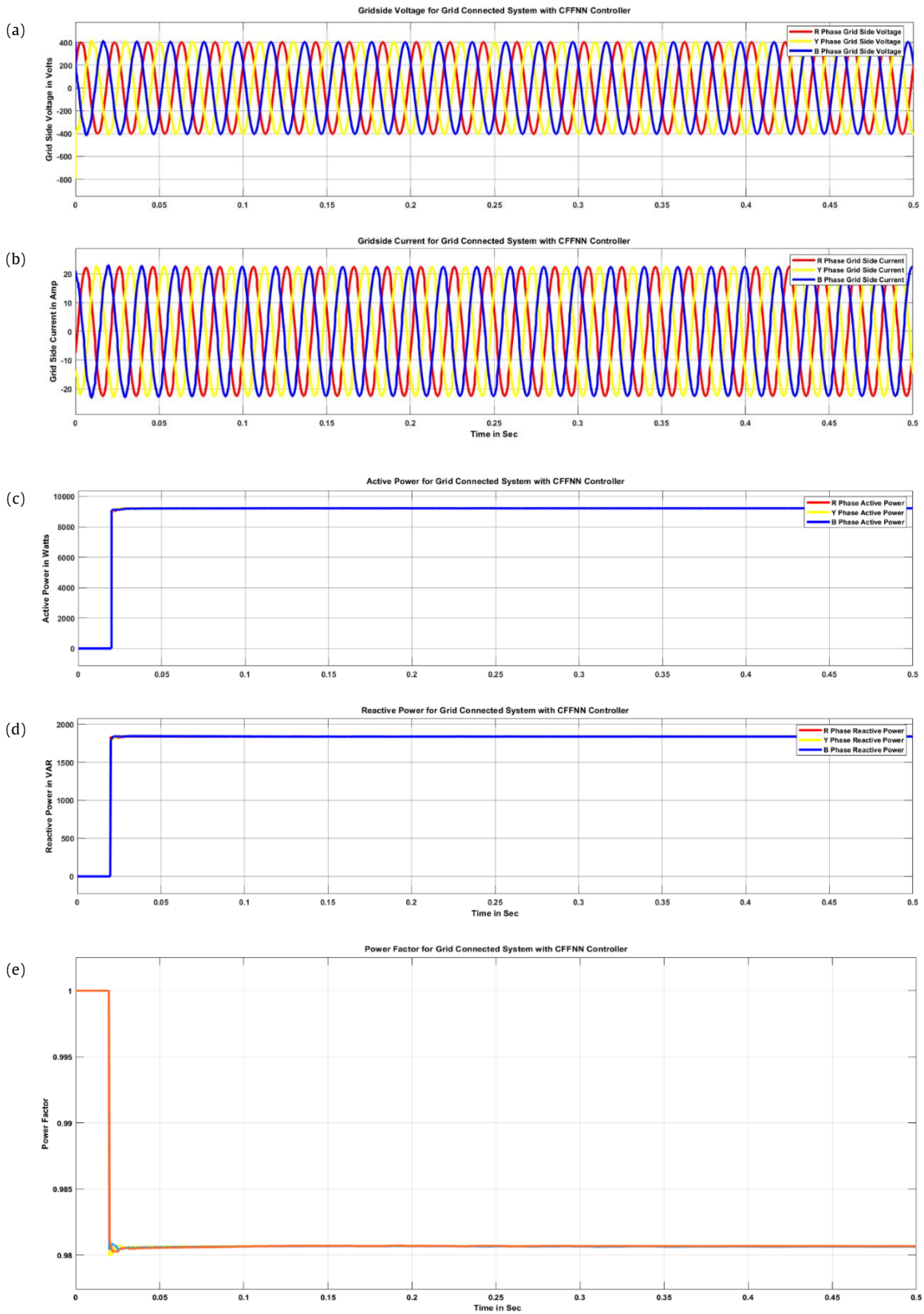


Figure 23. Three-phase load waveform of a grid-connected system with CFFNN control algorithm: (a) gridside voltage; (b) gridside current; (c) active power; (d) reactive power; and (e) power factor

Figure 24 and Figure 25 show the THD values of load voltage and current at the common coupling point (PCC) with the CFFNN algorithm at VSC, and the table with all topologies of load voltage and

current THD values for all phases is listed in Table 1. The power factor by using the CFFNN controller for a grid-connected system is 0.982 shown in Figure 23(e). Figures 24 and Figure 25 give the total

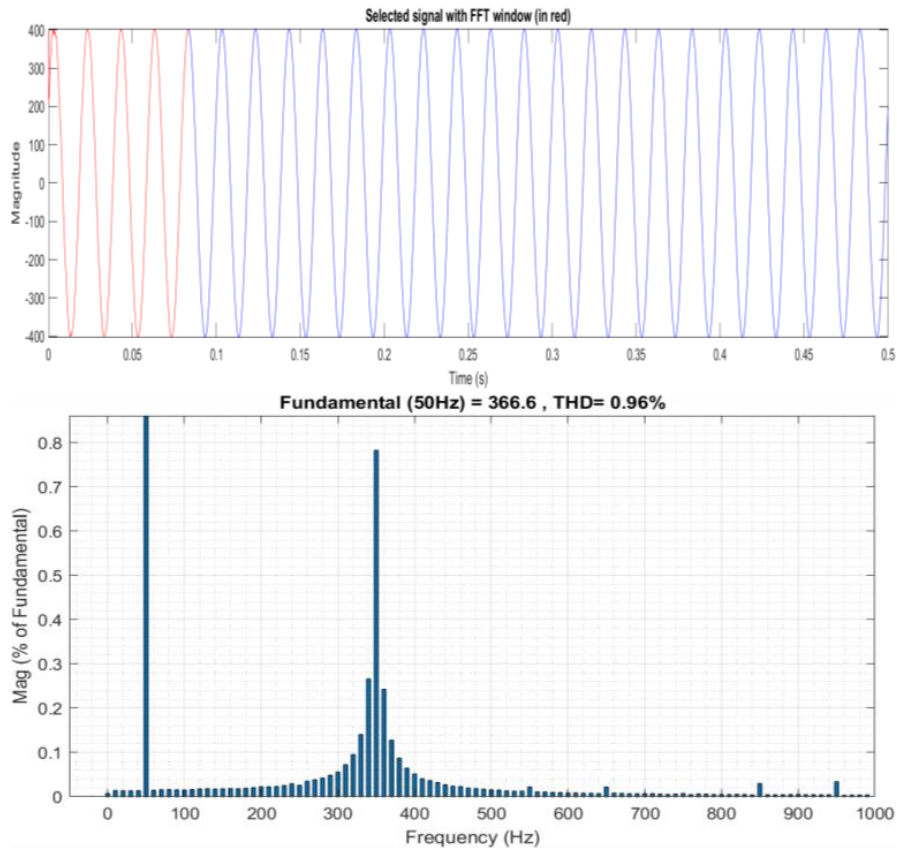


Figure 24. Load voltage THD at the common coupling of PV and power grid with CFFNN controller

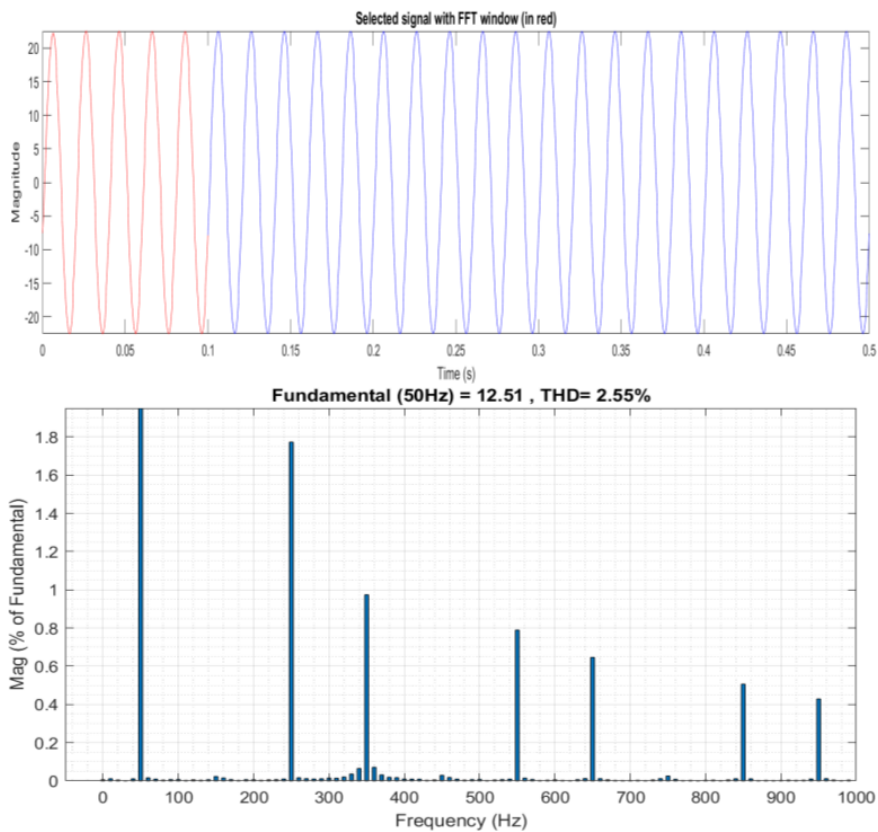


Figure 25. Load current THD at the common coupling of PV and power grid with CFFNN controller

harmonic distortion of load voltage and load current at different loading conditions like unbalanced and non-linear load for a standalone system in a specified time period with CFFNN current controller. From the figure, it is clear that the THD for load voltage is 0.96 %, and the load current is 2.55 %.

C. DNN controller for standalone system

Figure 26 demonstrate the overall performance of the suggested current regulator (load voltage, load current, active, reactive powers, and power factors) using the DNN algorithm for a standalone system.

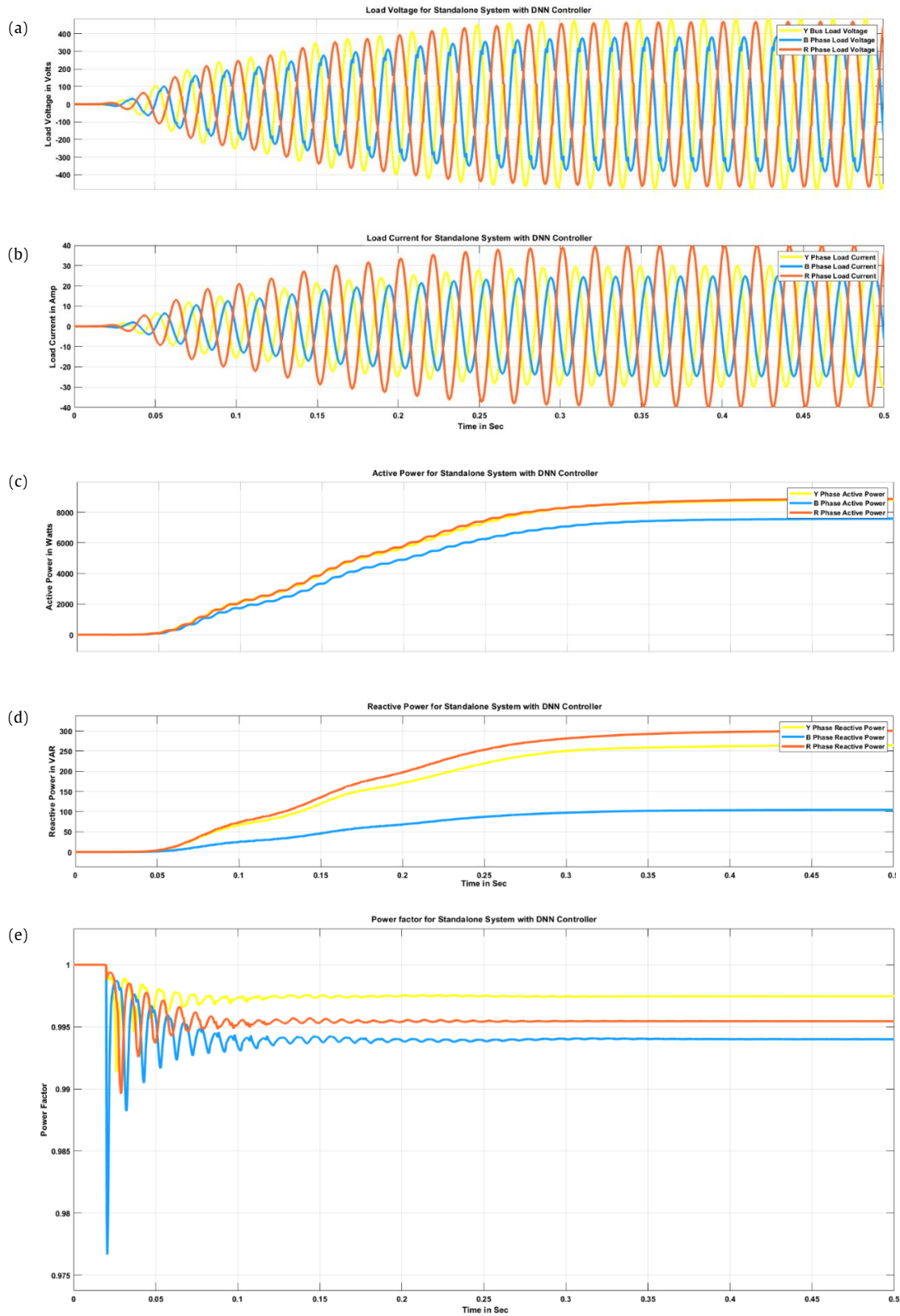


Figure 26. Three-phase load waveform of DNN controller for a standalone system: (a) load voltage; (b) load current; (c) active power; (d) reactive power; and (e) power factor

Figure 27 and Figure 28 give the THD of load voltage and load current for a standalone system with DNN. The power factor by using the DNN controller for a standalone system is 0.996, which is almost unity, as shown in Figure 26(e). Figures 27 and Figure 28 give the total harmonic distortion of

load voltage and load current at different loading conditions like unbalanced and non-linear load for a standalone system in a specified time period with DNN current controller. From the figure, it is clear that the THD for load voltage is 3.19 %, and the load current is 0.79 %.

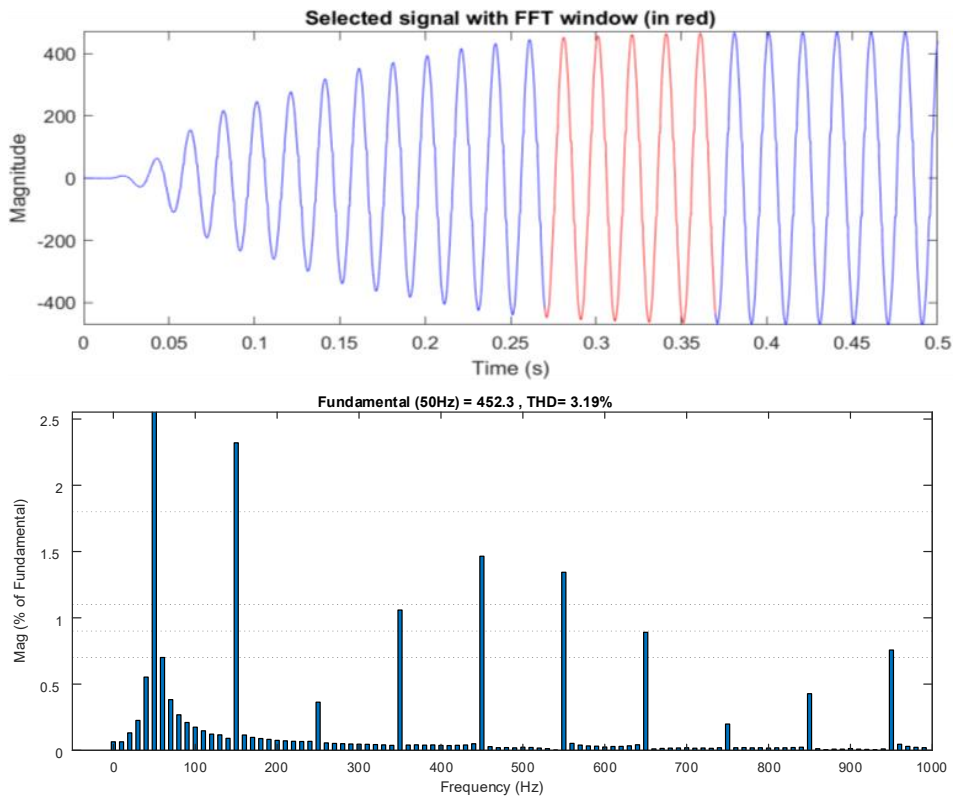


Figure 27. Load voltage THD for a standalone system with DNN controller

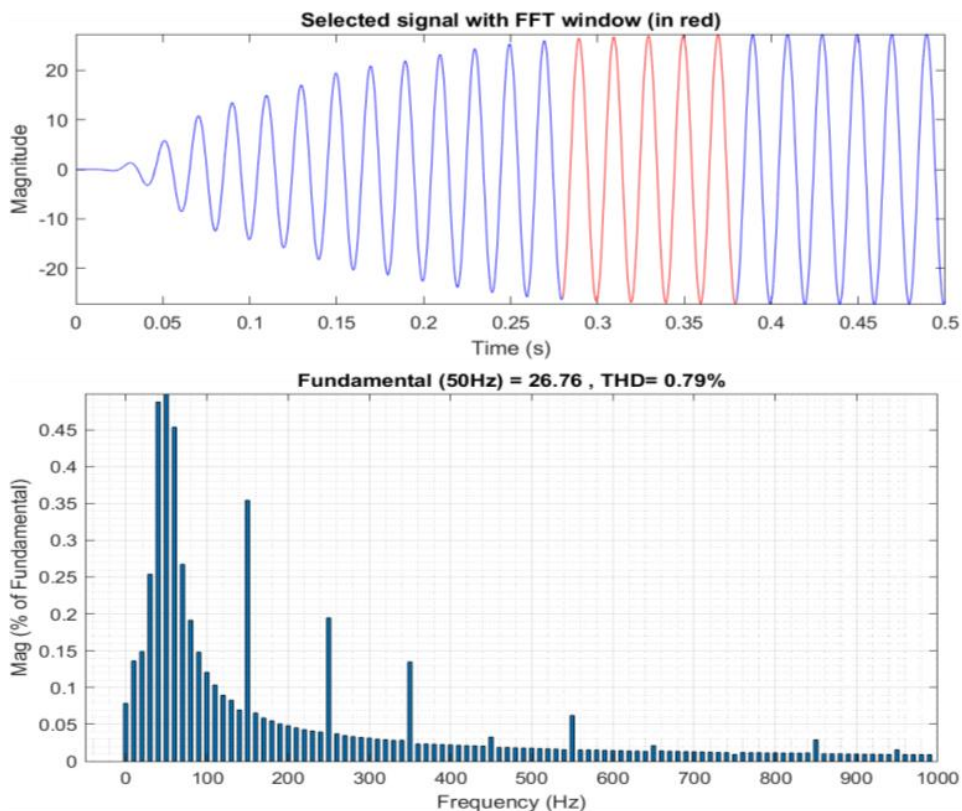


Figure 28. Load current THD for a standalone system with DNN controller

D. DNN controller for grid integrated PV system

The PV system's recommended DNN-based grid integration was built in a Matlab environment, as illustrated in Figure 15. More than 90,000 data points are employed to provide training (80 %), testing (10 %), and validation (10 %). The suggested system's best validation performance is 1.1225e-12 at epoch 3448, as shown in Figure 16. The suggested DNN algorithm for the current regulator's overall

performance was evaluated using the following parameters: training, validation testing, and overall results are shown in Figure 17. For grid synchronization, the developed current regulator algorithm was used on the suggested PV-connected inverter. The created current regulator algorithm has been applied in the planned CMLI for coordinating into the grid, and the grid-connected model's load voltage, current, active power, reactive power, and power factor are analyzed in Figure 29.

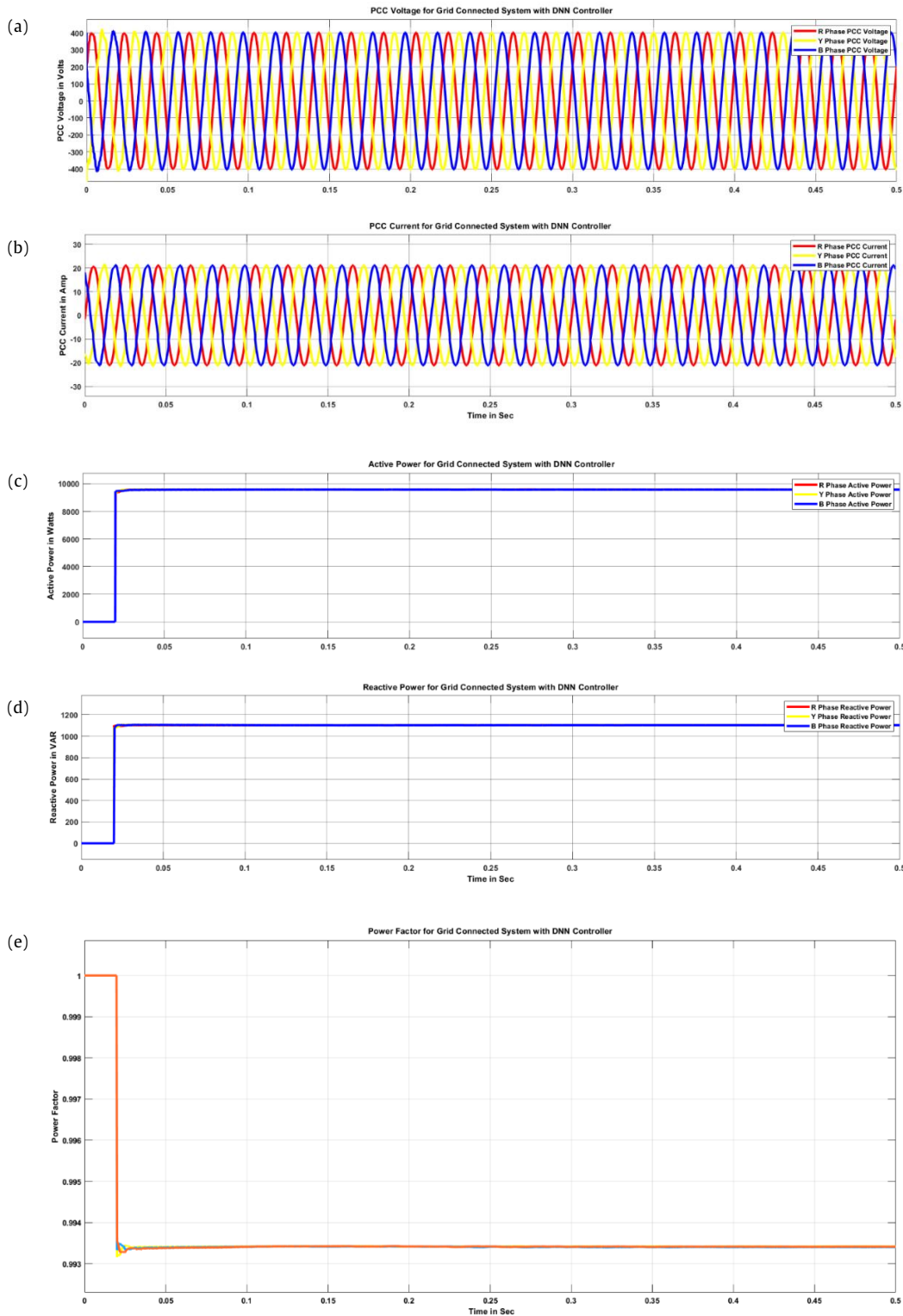


Figure 29. Three-phase load waveform of a grid-connected system with DNN controller: (a) PCC voltage; (b) PCC current; (c) active power; (d) reactive power; and (e) power factor

Figure 30 and Figure 31 show the THD values of load voltage and current at PCC with the CFFNN algorithm at VSC, and the table with all topologies of load voltage and current at PCC THD values for all

phases are listed in Table 1. The power factor by using DNN controller for a grid-connected system is 0.993, which is almost unity as shown in Figure 29(e). Figure 30 and Figure 31 give the total

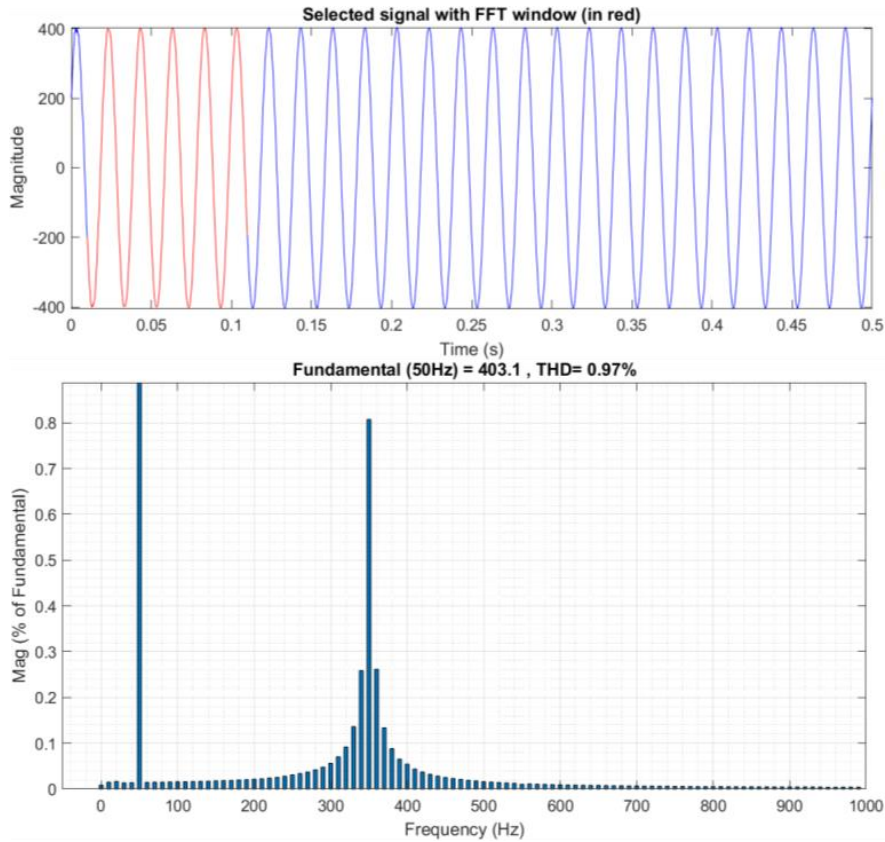


Figure 30. Load voltage THD at the common coupling of PV and power grid with DNN controller

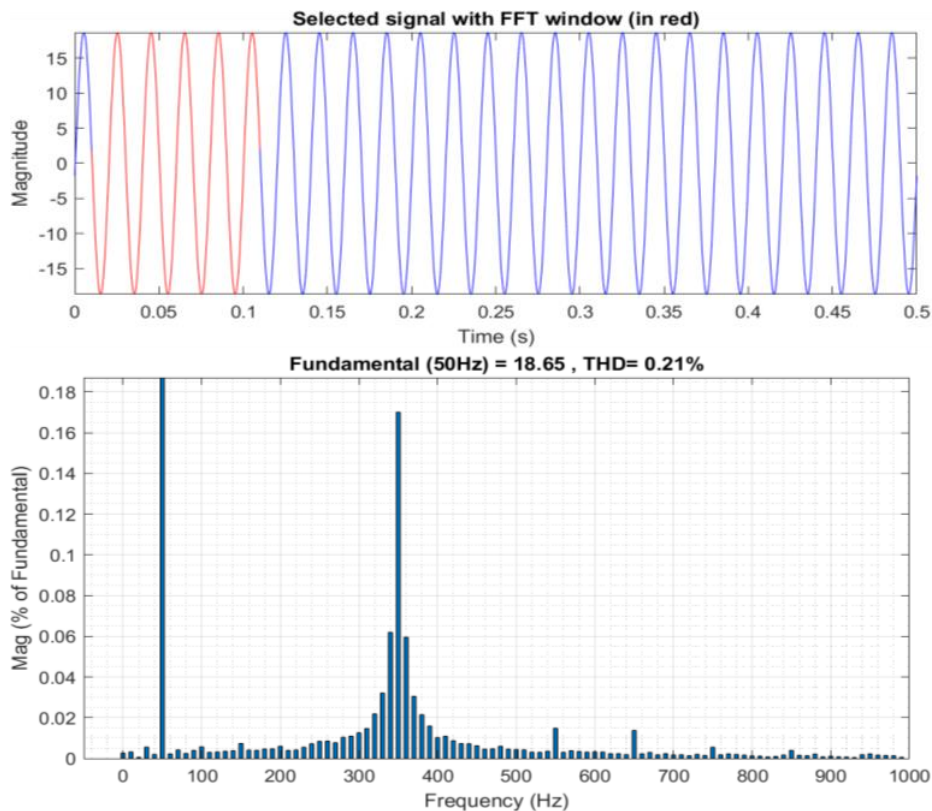


Figure 31. Load current THD at the common coupling of PV and power grid with DNN controller

Table 1.
THD comparison with nonlinear & unbalanced RL load

Controllers	Phase	Grid side voltage	Grid side current	Load side voltage	Load side current
Using PI controller	R	1.98 %	3.53 %	1.98 %	3.73 %
	Y	4.35 %	4.26 %	4.35 %	4.51 %
	B	2.41 %	3.71 %	2.41 %	3.93 %
Using fuzzy controller	R	1.98 %	3.42 %	1.98 %	3.74 %
	Y	4.37 %	4.15 %	4.37 %	4.4 %
	B	2.42 %	3.61 %	2.42 %	3.79 %
Using ANFIS controller	R	1.24 %	3.47 %	1.24 %	3.79 %
	Y	2.94 %	3.77 %	2.94 %	4.13 %
	B	1.73 %	3.39 %	1.73 %	3.71 %
Using CFFNN	R	0.96 %	2.55 %	0.96 %	2.66 %
	Y	2.39 %	3.44 %	2.39 %	3.63 %
	B	1.46 %	2.73 %	1.46 %	2.84 %
Using DNN	R	0.97 %	0.97 %	0.97 %	0.21 %
	Y	2.38 %	2.38 %	2.38 %	1.54 %
	B	1.41 %	1.41 %	1.41 %	1.74 %

Table 2.
Power factors of various control algorithms

S.No	Power factor for standalone system	Power factor for grid-connected system
CFFNN control algorithm	0.99	0.99
DNN control algorithm	0.99	≅ 1

harmonic distortion of load voltage and load current at different loading conditions like unbalanced and non-linear load for a grid-connected system in a specified time period with DNN current controller. From the figure, it is clear that the THD for load voltage is 0.97 %, and the load current is 0.21 %.

The reactive power of the system under standalone and grid-connected conditions for non-linear and unbalanced loads are given in Figures 20(d), 23(d), 26(d), and 29(d). From the figures, it is observed that for standalone systems, the required active power is supplied with a small-time delay of 0.3 s in the CFFNN control algorithm and 0.25 s of time delay in the DNN control algorithm. Table 1 represents the THD values of each phase of a standalone and grid-connected system with PI, Fuzzy, ANFIS, CFFNN, and DNN control algorithms with respect to non-linear and unbalanced resistive and inductive load. Table 2 represents the power factors of both control algorithms under standalone and grid-connected conditions with respect to non-linear and unbalanced RL loading conditions.

IV. Conclusion

In this study, the recommended DNN control method was applied to model a 10 kW PV system with a decreased switching 9-Level CMLI in Matlab. The system's performance was assessed under a range of operating situations, including active and reactive power, power factor, load voltage, and current THDs, and the model was simulated. The second portion of this study report focused on how different control algorithms are integrated and performed with PV systems. Last but not least, the suggested system was tested in a range of conditions, including unbalanced and non-linear. The time

needed to attain the voltage, current, and active power rating levels for standalone systems employing both CFFNN and DNN control algorithms takes 0.3 s and 0.25 s, respectively. According to the performance of the systems, the THD values of load voltage and current are 8.94 % and 8.54 % with CFFNN and 7.49 % and 7.07 % with the DNN controller, respectively. For grid-connected systems, neither the control algorithms have a time lag to reach the rated voltage, current, or active power, but the power factor values are 0.99 and approximately 1 for CFFNN and DNN controllers, respectively. PCC voltage THD values were 1.34 % and 2.58 % with CFFNN and 1.35 % and 0.82 % with DNN, respectively, excluding THD and DER connectivity to the grid. The DNN is used to virtually optimize unstructured data to obtain the best pulses for the cascaded inverter. The multiple layers in the DNN allow models to learn complex features more effectively and perform more intensive computational tasks, and it learns from its mistakes to obtain the optimized values. Deep learning algorithms may take into account diversity in learning characteristics to drastically reduce error margins across sectors and verticals. This is especially true when you consider deep learning algorithms' advantages over the limits of the traditional machine learning approach. When used in data science, deep learning can provide better and more efficient processing models. Accuracy and results are continuously improved because of its unsupervised learning capability. Additionally, it provides data scientists with clearer and more dependable analytical results. Due to its capacity to analyze enormous volumes of data and carry out numerous calculations in a time- and cost-efficient way, deep learning is extremely scalable.

Productivity (faster deployment/rollouts), modularity, and portability are all directly impacted by this. The efficacy of the suggested system is assessed using IEEE 519 simulation data. Based on the aforementioned study, it is obvious that the proposed DNN controller performs better in all aspects, including time to attain rated values, power factor, and THD calculation. As a result, the DNN is the ideal architecture for increasing the PQ of grid-connected PV systems under a variety of operating scenarios.

Declarations

Author contribution

All authors contributed equally as the main contributor of this paper. All authors read and approved the final paper.

Funding statement

This research did not receive any specific grant from funding agencies in the public, commercial, or not-for-profit sectors.

Competing interest

The authors declare that they have no known competing financial interests or personal relationships that could have appeared to influence the work reported in this paper.

Additional information

Reprints and permission: information is available at <https://mev.lipi.go.id/>.

Publisher's Note: National Research and Innovation Agency (BRIN) remains neutral with regard to jurisdictional claims in published maps and institutional affiliations.

References

- [1] S. Punna and U. B. Manthati, "Optimum design and analysis of a dynamic energy management scheme for HESS in renewable power generation applications," *SN Appl. Sci.*, vol. 2, no. 3, p. 495, Mar. 2020.
- [2] J. N. Bhanutej and R. C. Naidu, "A 7-level inverter with less number of switches for grid-tied PV applications," *Int. J. Adv. Technol. Eng. Explor.*, vol. 8, no. 78, pp. 631–642, May 2021.
- [3] K. Faqih, W. Primadi, A. N. Handayani, A. Prihartana, and K. Arai, "Smart grid photovoltaic system pilot scale using sunlight intensity and state of charge (SoC) battery based on Mamdani fuzzy logic control," *J. Mechatronics, Electr. Power, Veh. Technol.*, vol. 10, no. 1, pp. 36–47, Dec. 2019.
- [4] G. Maheswaran, M. Ettappan, T. Kavitha, and R. Senthil Kumar, "Effective DC-link voltage variation for renewable power application," *J. Phys. Conf. Ser.*, vol. 2027, no. 1, p. 012018, Sep. 2021.
- [5] G. K. Srinivasan, M. Rivera, V. Loganathan, D. Ravikumar, and B. Mohan, "Trends and challenges in multi-level inverter with reduced switches," *Electronics*, vol. 10, no. 4, p. 368, Feb. 2021.
- [6] S. Jayaraj, I. A. T. Parambaht, and B. Kunju, "Application of reinforcement learning algorithm for scheduling of microgrid," in *2019 Global Conference for Advancement in Technology (GCAT)*, Oct. 2019, pp. 1–5.
- [7] A. Manoranjan and C. C. A. Rajan, "Design and analysis of 31-level asymmetric cascaded H-Bridge Multilevel inverter with reduced number of switches," *Bull. Sci. Res.*, pp. 14–28, Oct. 2020.
- [8] M. Elamin, F. Elhassan, and M. A. Manzoul, "Comparison of deep reinforcement learning algorithms in enhancing energy trading in microgrids," in *2020 International Conference on Computer, Control, Electrical, and Electronics Engineering (ICCEEE)*, Feb. 2021, pp. 1–6.
- [9] M. H. Mandol, P. B. Shuvra, M. K. Hosain, F. Samad, and M. W. Rahman, "A novel single phase multilevel inverter topology with reduced number of switching elements and optimum THD performance," in *2019 International Conference on Electrical, Computer and Communication Engineering (ECCE)*, Feb. 2019, pp. 1–5.
- [10] N. Thombre, Ratika Singh Rawat, P. Rana, and Umashankar S, "New cost effective cascaded twenty one level asymmetrical inverter with reduced number of switches and DC sources," in *2014 International Conference on Advances in Electrical Engineering (ICAEE)*, Jan. 2014, pp. 1–5.
- [11] C. K. Kishore, K. Balaji, and J. Madhavan, "Modified cascaded switched diode multilevel inverter with multiple outputs and reduced harmonic content," in *2019 1st International Conference on Innovations in Information and Communication Technology (ICIICT)*, Apr. 2019, pp. 1–4.
- [12] M. A. Hosseinzadeh, M. Sarbanzadeh, M. Rivera, J. Munoz, A. Villalon, and C. Munoz, "New single-phase asymmetric reduced multilevel inverter based on switched-diode for cascaded multilevel inverters," in *2019 IEEE International Conference on Industrial Technology (ICIT)*, Feb. 2019, pp. 1494–1499.
- [13] L. Wang, Q. H. Wu, and W. Tang, "Novel cascaded switched-diode multilevel inverter for renewable energy integration," *IEEE Trans. Energy Convers.*, vol. 32, no. 4, pp. 1574–1582, Dec. 2017.
- [14] V. Narasimhulu, D. V. Ashok Kumar, and C. Sai Babu, "Computational intelligence based control of cascaded H-bridge multilevel inverter for shunt active power filter application," *J. Ambient Intell. Humaniz. Comput.*, Jan. 2020.
- [15] B. A. Farooqi, M. R. Bin Ahmad, and M. Ali, "Analysis of interconnected configuration for penetration of distributed generation," *Int. J. Adv. Technol. Eng. Explor.*, vol. 8, no. 74, pp. 1–11, Jan. 2021.
- [16] C. Lassetter, E. Cotilla-Sanchez, and J. Kim, "A learning scheme for microgrid reconnection," *IEEE Trans. Power Syst.*, vol. 33, no. 1, pp. 691–700, Jan. 2018.
- [17] V. Narasimhulu, D. V. Ashok Kumar, and C. Sai Babu, "Recital analysis of multilevel cascade H-bridge based active power filter under load variation," *SN Appl. Sci.*, vol. 1, no. 12, p. 1621, Dec. 2019.
- [18] H.-Q. Deng, J. Luo, C.-C. Li, P.-Q. Li, and R.-J. Zheng, "Preventive control strategy of cascading fault considering safety and economy," *J. Electr. Comput. Eng.*, vol. 2021, pp. 1–12, Oct. 2021.
- [19] J. Yu, Z. Gang, M. Peng, D. Song, and M. Liu, "Power-matching based SOC balancing method for cascaded H-bridge multilevel inverter," *CPSS Trans. Power Electron. Appl.*, vol. 5, no. 4, pp. 352–363, Dec. 2020.
- [20] M. Rupesh and T. S. Vishwanath, "Fuzzy and ANFIS controllers to improve the power quality of grid connected PV system with cascaded multilevel inverter," *Int. J. Electr. Electron. Res.*, vol. 9, no. 4, pp. 89–95, Dec. 2021.
- [21] R. Muhida, N. H. Mohamad, A. Legowo, R. Irawan, and W. Astuti, "Maximum power point tracking of photovoltaic system for traffic light application," *J. Mechatronics, Electr. Power, Veh. Technol.*, vol. 4, no. 1, pp. 57–64, Jul. 2013.